DEUTSCHES ELEKTRONEN-SYNCHROTRON
Ein Forschungszentrum der Helmholtz-Gemeinschaft

DESY 19-146
IFIC/19-35
KEK Preprint 2019-22
SLAC-PUB-17467
arXiv:1908.11299
August 2019

Tests of the Standard Model at the International Linear Collider

LCC Physics Working Group

ISSN 0418-9833

NOTKESTRASSE 85 - 22607 HAMBURG

To be sure that your reports and preprints are promptly included in the HEP literature database
send them to (if possible by air mail):

DESY Zentralbibliothek Notkestraße 85 22607 Hamburg Germany	DESY Bibliothek Platanenallee 6 15738 Zeuthen Germany

DESY 19-146, IFIC/19-35
KEK Preprint 2019-22
SLAC-PUB-17467
August, 2019

Tests of the Standard Model at the International Linear Collider

LCC Physics Working Group

Keisuke Fujii[1], Christophe Grojean[2,3], Michael E. Peskin[4] (Conveners); Tim Barklow[4], Yaunning Gao[5], Shinya Kanemura[6], Hyungdo Kim[7], Jenny List[2], Mihoko Nojiri[1,8], Maxim Perelstein[9], Roman Pöschl[10], Jürgen Reuter[2], Frank Simon[11], Tomohiko Tanabe[12], James D. Wells[13], Jaehoon Yu[14]; Junping Tian[12], Taikan Suehara[15], Marcel Vos[16], Graham Wilson[17]; James Brau[18], Hitoshi Murayama[8,19,20] (ex officio)

ABSTRACT

We present an overview of the capabilities that the International Linear Collider (ILC) offers for precision measurements that probe the Standard Model. First, we discuss the improvements that the ILC will make in precision electroweak observables, both from W boson production and radiative return to the Z at 250 GeV in the center of mass and from a dedicated GigaZ stage of running at the Z pole. We then present new results on precision measurements of fermion pair production, including the production of b and t quarks. We update the ILC projections for the determination of Higgs boson couplings through a Standard Model Effective Field Theory fit taking into account the new information on precision electroweak constraints. Finally, we review the capabilities of the ILC to measure the Higgs boson self-coupling.

[1] *High Energy Accelerator Research Organization (KEK), Tsukuba, Ibaraki, JAPAN*
[2] *DESY, Notkestrasse 85, 22607 Hamburg, GERMANY*
[3] *Institut für Physik, Humboldt-Universität zu Berlin, 12489 Berlin, GERMANY*
[4] *SLAC, Stanford University, Menlo Park, CA 94025, USA*
[5] *Department of Physics, Peking University, Beijing 100871, CHINA*
[6] *Department of Physics, Osaka University, Machikaneyama, Toyonaka, Osaka 560-0043, JAPAN*
[7] *Dept. of Physics and Astronomy, Seoul National Univ., Seoul 08826, KOREA*
[8] *Kavli Institute for the Physics and Mathematics of the Universe, University of Tokyo, Kashiwa 277-8583, JAPAN*
[9] *Laboratory for Elementary Particle Physics, Cornell University, Ithaca, NY 14853, USA*
[10] *LAL, Centre Scientifique d'Orsay, Université Paris-Sud, F-91898 Orsay CEDEX, FRANCE*
[11] *Max-Planck-Institut für Physik, Föhringer Ring 6, 80805 Munich, GERMANY*
[12] *ICEPP, University of Tokyo, Hongo, Bunkyo-ku, Tokyo, 113-0033, JAPAN*
[13] *Michigan Center for Theoretical Physics, University of Michigan, Ann Arbor, MI 48109, USA*
[14] *Department of Physics, University of Texas, Arlington, TX 76019, USA*
[15] *Department of Physics, Kyushu University, Fukuoka, JAPAN*
[16] *IFIC, University of Valencia, Valencia, SPAIN*
[17] *Department of Physics and Astronomy, University of Kansas, Lawrence, KS 66045, USA*
[18] *Center for High Energy Physics, University of Oregon, Eugene, Oregon 97403-1274, USA*
[19] *Department of Physics, University of California, Berkeley, CA 94720, USA*
[20] *Theoretical Physics Group, Lawrence Berkeley National Laboratory, Berkeley, CA 94720, USA*

Contents

1 Introduction

Given the central role of the Higgs boson in the Standard Model of particle physics, the detailed study of the properties of the Higgs boson will be a major goal of future particle physics experiments. The planned future running of the Large Hadron Collider will improve our knowledge of the Higgs boson, as documented in the report [1] on the prospects for Higgs studies in its high-luminosity phase. However, a true high-precision understanding of the Higgs boson, capable of discovering new physics through the Higgs boson over a wide range of models, has an even more challenging requirement: It demands that we push the uncertainties in Higgs boson couplings below the 1% level [2]. This will require studies of Higgs boson production at an e^+e^- collider. A number of e^+e^- Higgs factories have been proposed and are now in various stages of readiness for construction.

It has recently become clear that the best way to extract the values of the couplings of the Higgs boson from experimental observables is to make use of Standard Model Effective Field Theory (SMEFT) [3–6]. In this method, deviations in the Higgs couplings from the predictions of the Standard Model (SM) are parametrized by the addition to that model of the most general set of dimension-6 gauge-invariant operators. This is a very general parametrization that can incorporate the effects of almost any type of new physics that can modify the SM at high energies. The SMEFT method gains its power from unifying constraints on the SM that come from many sources, including not only Higgs measurements but also measurements of precision electroweak observables, triple gauge boson couplings, and two-fermion production processes including top quark production. One of the advantages of e^+e^- colliders is that they offer a large number of well-characterized, independent observables, enough to determine independently each coefficient for the full set of operators that contribute to Higgs boson processes. The number of observables becomes even larger, so that the fit is actually overconstrained, with the use of polarised beams. Using this method, we can extract the Higgs boson couplings from experimental observables in e^+e^- collisions with no model-dependent assumptions other than the validity of the SMEFT itself.

The goal of this paper is to explain systematically the determination of these SMEFT coefficients at the e^+e^- Higgs factory that we consider closest to realization—the International Linear Collider (ILC) in Japan. We will present estimates for the precision with which all relevant SMEFT parameters will be determined in the proposed ILC program. As has been explained in previous expositions on the ILC, these estimates come from full-simulation analyses based on detailed detector models [7,8]. Thus, we have very high confidence that the precision we claim for these measurements can be realized in practice when the ILC is constructed.

Our projections for the ILC uncertainties in precision electroweak observables and our updated projections for Higgs boson couplings are presented in the tables in

Appendix A.

The outline of this paper is as follows: In Section 2, we will describe the expected run plan of the ILC. The minimal plan for the ILC includes running at 250 GeV, 350 GeV, and 500 GeV with polarised beams. The ILC is also capable of a run at the Z pole ("GigaZ") with minimal modification. By extending the length of the linacs, the ILC can run at 1 TeV with the same accelerator technology. The machine parameters for all of these settings have been described previously [8, 9]. In Section 2, we will review the plans for each stage, giving for each the expected integrated luminosities and calendar durations.

Precision measurements at e^+e^- colliders depend crucially on a precise knowledge of the beam parameters and the detector performance. Especially for precision electroweak measurements, large event samples are not useful unless one can ensure that the experimental systematic errors are sufficiently small. Linear colliders such as the ILC offer the possibility of longitudinal polarisation both for the electron and positron beams. We will see that the use of polarisation allows us to design measurements in which the systematic errors on beam parameters are the dominant ones that must be considered. In Section 3, we will explain how the rather ambitious goals this requires for the systematic errors on beam polarisations and energies will be met.

Following this introduction, we present our survey of ILC physics results. We have previously presented detailed discussions of the measurements of single-Higgs production and W boson couplings in [8]. Here, we will only give updates to these measurements. Our main focus will be on precision electroweak observables and observables of fermion pair production.

We begin in Section 4 with a discussion of the W boson mass and width. We will describe the measurement of the mass of the W boson from kinematic fitting to $e^+e^- \to W^+W^-$ events at 250 GeV. Section 4 will also briefly describe the measurement of the W mass that would be possible in a dedicated run at the WW threshold.

Section 5 gives an introduction to the Z pole observables that we will discuss in this report. The best possible ILC measurements of precision electroweak parameters will be obtained from a dedicated GigaZ run at the Z pole. However, data at 250 GeV taken as a part of the Higgs boson study will already markedly improve our knowledge of precision electroweak observables beyond what is known today. Section 6 will describe the measurement of Z-fermion couplings from the radiative return process $e^+e^- \to Z\gamma$ at 250 GeV. Section 7 will describe the GigaZ program and the further improvement of precison electroweak measurements that will be possible there. The ILC expectations for precision electroweak measurements are summarized in Table 9 in Appendix A.

We then turn to the precision measurement of fermion pair production at 250 GeV and at higher energies. Section 8 will present the expectations for ILC precision

tests of of $e^+e^- \to f\overline{f}$ cross sections, including constraints on s-channel Z' bosons. This section will also describe the measurement of four-fermion contact interactions at the ILC. These contact interactions may, in principle, depend on fermion flavor and helicity. Current limits from the LHC are given in schemes restricted by model-dependent relations among these couplings. At an e^+e^- collider with polarised beams, each individual coefficient of a contact interaction can be measured independently.

Section 9 will discuss special aspects of the pair-production of bottom and top quarks. The treatment of these heavy quarks in SMEFT is especially complicated, requiring 17 independent operators beyond those appropriate for processes with light flavors. In this section, we will explain how these operator coefficients can be measured in the ILC runs at 250 GeV, 500 GeV, and 1 TeV. The various coefficients can be completely disentangled in a model-independent way [10,11]. This study is interesting in its own right, because the precision study of the top quark can hold its own clues to possible new physics. But, also, these results allow a precise determination of the top quark Yukawa coupling in a way that is free of model-dependent assumptions needed for the extraction of this coupling at hadron colliders.

Section 10 will put all of these pieces together and present the expected results from the global SMEFT fits for Higgs boson couplings that will be possible at the 250 GeV, 500 GeV, and 1 TeV stages of the ILC. This program is capable of bringing the uncertainty on all major Higgs couplings below the 1% level. We also discuss the effect on this analysis of higher-precision results from GigaZ. The ILC expectations for the measurement of Higgs boson couplings are summarized in Table 10 in Appendix A.

Section 11 will describe the determination of the Higgs self-coupling at the ILC, first directly from the measurement of double Higgs boson production at 500 GeV and 1 TeV, and also indirectly by the inclusion of a parameter for the Higgs self-coupling in the SMEFT fit. We will show that the ILC at 1 TeV will offer multiple determinations of the Higgs self-coupling. The combination will give a precision better than 10%, determined in a manner that is free of model-dependent assumptions on the nature of new physics.

2 ILC accelerator run plan and options

To discuss the capabilities of the ILC, it is first necessary to specify the run plan in terms of energies, integrated luminosities, and polarisation settings. The current proposed run plan for the ILC raises the CM energy in stages, with runs at 250 GeV, 350 GeV, and 500 GeV. It is also possible to run the ILC at the Z pole with minimal modification. By lengthening the ILC tunnel, improving the gradient of the superconducting RF cavities, or a combination of these, it is possible to run the ILC

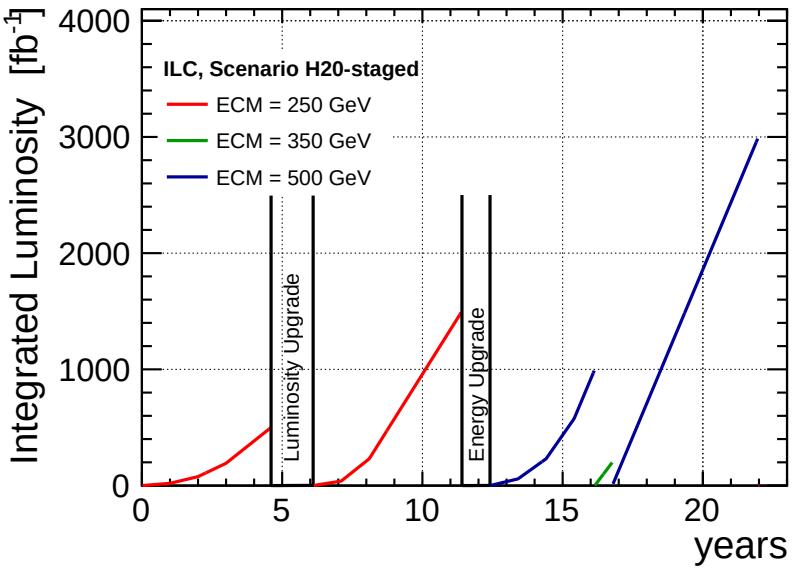

Figure 1: The nominal 22-year running program for the staged ILC, starting operation at 250 GeV [8].

at a CM energy of 1 TeV. All of these possibilities have been described, together with the necessary machine parameters, in the previous ILC reports [8, 9, 12, 13].

2.1 Minimal plan

The currently proposed run plan, in terms of energy and luminosity, is illustrated in Fig. 1 [8]. The initial running of the ILC will be at a CM energy of 250 GeV with bunch trains of 1312 e^- or e^+ bunches per linac pulse, ramping up to an instantaneous luminosity of $1.35 \times 10^{34}\text{cm}^{-2}\text{sec}^{-1}$. After 6 years, additional RF power will be added, increasing the number of bunches per linac pulse to 2625 and doubling the instantaneous luminosity. This is a relatively inexpensive change, estimated at 8% of the initial ILC cost. It is referred to in the figure as the "Luminosity Upgrade". After reaching a total integrated luminosity of 2 ab^{-1}, the linacs would be lengthened to provide a CM energy of 500 GeV. This is referred to in the figure as the "Energy Upgrade". In fact, if funds are available, most of this upgrade could be prepared in parallel with physics running at 250 GeV. The extended machine would then ramp up to an instantaneous luminosity of $3.6 \times 10^{34}\text{cm}^{-2}\text{sec}^{-1}$ and acquire 4 ab^{-1} of data, with a brief interval of running at 350 GeV to measure the top quark mass with high precision. The luminosity of a linear collider naturally rises approximately linearly with CM energy, making it easier to acquire larger luminosity samples as the energy is increased.

	E_{CM} (GeV)	$\int \mathcal{L}$ (fb^{-1})	fraction with sign$(P(e^-), P(e^+)) =$ $(-+)$	$(+-)$	$(--)$	$(++)$
ILC250	250	2000	45%	45%	5%	5%
ILC350	350	200	67.5%	22.5%	5%	5%
ILC500	500	4000	40%	40%	10%	10%
GigaZ	91.19	100	40%	40%	10%	10%
ILC1000	1000	8000	40%	40%	10%	10%

Table 1: CM energy, integrated luminosity, and polarisation fractions for the stages of ILC discussed in this report. In all cases, the magnitude of the e^- polarisation is taken to be 80% and the magnitude of the e^+ polarisation is taken to be 30%, except that, at ILC1000, 20% e^+ polarisation was used in the studies quoted.

The ILC is designed to provide significant polarisation for both the electron and positron beams. We expect $\pm 80\%$ polarisation for the electron beam and $\pm 30\%$ polarisation for the positron beam. Beam polarisation plays an important role in the ILC physics, both in producing additional observables with significant physics information and in controlling systematic errors. The importance of polarisation at the ILC is discussed in detail in [14, 15]. Thus, for each operating energy of the ILC, one must also specify the fraction of time that will be spent in each of the four possible polarisation states. Our baseline choices are given in Table 1. Note that the physics studies at 1 TeV, described below, assumed a positron polarisation of $\pm 20\%$.

The full calendar duration of the minimal ILC plan shown in Fig. 1 is 22 years. However, the plan for the ILC allows additional stages of running either interleaved with those just described or carried out after the end of the program. In this report, we will discuss results for a GigaZ stage at Z resonance and for an ILC stage at 1 TeV. The GigaZ program, in particular, could be carried out within or after the 250 GeV stage or within the 500 GeV stage, whenever its physics results are deemed to be required. In the following, we will refer to the stages of the ILC as ILC250, ILC350, *etc.*, following the nomenclature of Table 1.

2.2 GigaZ

Although a physics run at the Z pole is not part of the minimum baseline run plan of the ILC, it has always been considered as an important option which should not be obstructed by the accelerator design. In particular, the GigaZ operation was considered in the 2015 study by the Joint Working Group on ILC Beam Parameters [9]. That group recommended the following run scenario as the canonical one for physics studies: The integrated luminosity should be taken as $100\,\text{fb}^{-1}$. Both beams are assumed to be polarised, with the polarisation fractions as in Table 1.

	sign$(P(e^-), P(e^+)) =$				
	$(-,+)$	$(+,-)$	$(-,-)$	$(+,+)$	sum
luminosity [fb^{-1}]	40	40	10	10	
$\sigma(P_{e^-}, P_{e^+})$ [nb]	60.4	46.1	35.9	29.4	
Z events [10^9]	2.4	1.8	0.36	0.29	4.9
hadronic Z events [10^9]	1.7	1.3	0.25	0.21	3.4

Table 2: Integrated luminosities per beam helicity configuration for Z pole running of the ILC, along with the corresponding cross sections and numbers of produced Z's.

Table 2 shows the resulting distribution of the luminosity onto the four polarisation sign configurations, along with the corresponding polarised cross sections for $|P_{e^-}| = 80\%$ and $|P_{e^+}| = 30\%$ and the number of produced (hadronic) Z events. These have been calculated based on the values for the unpolarised peak hadronic cross section including QED radiative corrections, $\sigma = 30\,\text{nb}$ [17], and the left-right asymmetry, $A_{LR} = (A_e) = 0.1515$ [16]. The last column gives the total number of (hadronic) Z events summed over all data sets. Thus, "GigaZ" is actually nearly 5 (3.5) $\times 10^9$ Z events in all (hadronic) decay modes.

The presence of four data sets of different polarisation signs allows a very precise and robust determination of the left-right asymmetry of the Zee coupling, as we will describe in Section 7 [14].

There are different schemes for implementing the Z pole operation at the ILC, depending on the machine stage at the time that this run is scheduled. The actual running time required to collect the GigaZ event sample depends on this implementation and can range between 1 and 3 years. None of the possible implementations has been studied at a level of detail comparable to the ILC baseline. Therefore, the estimates in this report are very conservative. They are expected to improve with further optimisation of the machine design.

Originally, the implementation of the GigaZ option was studied for the case of the 500 GeV machine [18]. With that as a starting point, the electron linac would be operated at 5+5 = 10 Hz, alternating between pulses accelerated to $M_Z/2$ for collisions and pulses accelerated to 150 GeV for positron production. Higher luminosities could be reached by splitting the electron linac into separate halves devoted to these two purposes.

Recently, the situation was reconsidered assuming that the GigaZ run would be done after the first stage of the ILC at 250 GeV [19]. Without assuming the installation of any additional cryogenic power, the electron linac could be operated at 3.7 Hz + 3.7 Hz, alternating between acceleration to $M_Z/2$ and to the nominal 125 GeV. This proposal also takes advantage of a recent optimisation of the machine design,

allowing for a smaller horizontal emittance achieved in the damping rings. After a preliminary study of the emittance growth along the linacs and of the final focus system, an instantaneous luminosity of about $2.1 \times 10^{33}\text{cm}^{-2}\text{s}^{-1}$ seems achievable without major modifications. This luminosity estimate does not assume the 250 GeV luminosity upgrade, and so correspondes to 1315 bunches per pulse. If the GigaZ run is done after the luminosity upgrade, to 2625 bunches per pulse, this would double the GigaZ luminosity to about $4.2 \times 10^{33}\text{cm}^{-2}\text{s}^{-1}$. With the standard ILC assumption of 1.6×10^7 s of running per year, the $100\,\text{fb}^{-1}$ assumed in the physics studies would correspond to about 3.0 years if done before the luminosity upgrade, or about 1.5 years if done afterward. If improvement of the precision electroweak measurements became an important issue, a longer run could be scheduled. In a 4 year run (as requested for FCC-ee), three times as many Z events as assumed above could be collected.

Significant further increases of the luminosity could be expected from a more modern design of the damping rings, aiming for a smaller longitudinal emittance as well as for tighter focusing, and from a better design of the Beam Delivery System with a larger aperture of the final focus quadrupoles and a larger momentum band width. To put these improvements on a solid footing, additional studies are needed. Therefore we currently do not increase the assumed size of the data set beyond $100\,\text{fb}^{-1}$ for physics studies, although the above discussion shows that larger data sets could possibly be obtained if the physics need arises.

2.3 1 TeV

The ILC can be upgraded in energy to 1 TeV using current superconducting RF technology. Machine parameters for this upgrade were presented in the ILC TDR [12], Chapter 12.2. The machine evolution needed is also described in Sec. 2.4.1 of [8]. Running of the ILC at 1 TeV looks far enough into the future that a new generation of accelerator technology will likely have come into play. However, many proposals presented to the 2019 European Strategy for Particle Physics are extrapolated over such long time scale – for example, FCC presents a 50-year program – so our projections for 1 TeV should be taken in the same spirit.

The run plan for 1 TeV operation with current technology was described in Sec. 7 of [9]. There, it is proposed to acquire a total of 8 ab^{-1} of data. Both beams are assumed to be polarised, with polarisations of 80% and 20% for the electrons and positrons, respectively, with polarisation fractions as detailed in Table 1. Since the luminosity of a linear collider naturally increases with the CM energy, the calendar time for this run would be similar to that for the 4 ab^{-1} run at 500 GeV, that is, 7–8 years.

The ILC at 1 TeV has interesting capabilities to search for new color-singlet par-

ticles. It will extend the search reach for pair-production of dark matter particles, using the mono-photon signature, and for electroweakinos and similar particles with compressed spectrum to interesting and relevant regions of parameter space. In this report, however, we will concentrate on the expected results in Higgs boson physics.

By the end of the 500 GeV ILC program, we hope that a new high-gradient accelerator technology will be ready to form the basis of a successor to the ILC. Ideas for electron acceleration at a few GeV/m that are now being investigated would produce an electron collider in the same tunnel as the ILC at multi-10 TeV energies. We see this as the true long-term future of the ILC laboratory. However, the 1 TeV run of the ILC with current technology is something that we can propose now and investigate with our current analysis tools.

3 Measurement of polarisation and beam energy at the ILC

Precise knowledge of the electron and positron beam energy and polarisation is essential for many measurements at the ILC, and in particular for the Higgs and electroweak program. For both energy and polarisation, the final values will be obtained by combining measurements from dedicated beam instrumentation with information extracted from the electron-positron collisions themselves. The beam instruments — polarimeters and energy spectrometers [20] — provide fast measurements which can resolve the time-dependence of beam parameters during a run, while the collision data provide the long-term overall scale calibration. In the following, we will summarize the state-of-the-art concepts for polarimetry and beam energy measurement which lead to the estimates of the associated systematic uncertainties used in the remainder of this document.

3.1 Beam polarisation measurement

The polarisation of the electron and positron beams will be measured by Compton polarimeters located about 1.8 km before and 100 m behind the e^+e^- interaction point (IP). These polarimeters have been designed to measure the "instantaneous" longitudinal polarisations at the polarimeter locations with negligible statistical uncertainties and a systematic uncertainty not larger than $\Delta P/P = 0.25\%$ [21, 22]. Optionally, the transverse polarisation components could also be measured [23].

These polarimeter measurements need to be corrected for the spin transport through the magnets of the Beam Delivery System as well as for the depolarisation in the collisions themselves. These effects have been investigated in detail for ILC500, with the result that they can be controlled to the level of 0.1% [24], provided that both the relative alignment of the orbit between the e^+e^- IP and the polarimeter

locations as well as other beam parameters (energy, intensity, emittance, β function at IP) are sufficiently well known. With such corrections, the luminosity-weighted long-term average of the polarisation at the e^+e^- IP can then in principle be derived from the polarimeter measurements.

The polarisations of the electron and positron beams can also be measured from the observed e^+e^- cross sections. What makes this strategy effective is that, at energies above the Z pole, well-understood processes such as forward W pair production have cross sections with strong polarisation-dependence. The estimate of polarisation from these measurements does not rely on the modeling of the accelerator parameters, but high precision is obtained only by integrating over long periods, which washes out time-dependent variations. Therefore, the extraction of the polarisation from collision data and the measurements by the polarimeter complement one another and will be combined to achieve the ultimate level of precision.

The extraction of the luminosity-weighted long-term average polarisations from collision data has been the subject of many studies. The latest status can be found in [25]. Observations to note are:

- It is important to have four independent beam settings with positive and negative values for both beam polarisations P_{e^-} and P_{e^+}. It is not sufficient to assume that the absolute value of the polarisation stays the same when the polarisation is reversed, as in the modified Blondel scheme [26, 27]. Instead, it is necessary to correct the results from the Blondel scheme based on the polarimeter measurements, and it is this effect that actually limits the final precision [25].

- When the total and differential cross sections for 2- and 4-fermion processes are combined to extract the four polarisation parameters, these parameters can be determined to a few parts in 10^4 [25], provided that the efficiencies and purities of the event selections can be controlled at the per mille level. This justifies the estimates used in this paper that the relative systematic errors on left-right asymmetries due to the uncertainty of the beam polarisations is about 3×10^{-4} at $\sqrt{s} = 250\,\mathrm{GeV}$. At the Z pole, no 4-fermion processes will be available; therefore we expect larger systematic uncertainties of 5×10^{-4}.

- We are currently developing a superior method for the estimate of polarisation uncertainties: the inclusion of the polarisation values as nuisance parameters in the extraction of the main observables in e^+e^- cross section measurements. This has been done routinely in the projections for triple gauge coupling precisions [25, 28], and has recently been started also for the extraction of other electroweak parameters [25]. In a simultaneous extraction of the beam polarisations at the ILC250, the total unpolarised cross sections and the left-right asymmetries of various 2- and 4-fermion processes using a fit to the total and dif-

ferential cross section measurements of these processes, precisions of 4.3×10^{-4} and 5×10^{-4} have been obtained for $A_{LR}(e^+e^- \to q\bar{q})$ and $A_{LR}(e^+e^- \to l^+l^-)$, respectively. These numbers, which combine the statistical uncertainty and the uncertainty due to the finite knowledge of the polarisation, are even better than the results we present later in this document. However, since this study is not yet based on full simulation, we only take it here as additional support that the precisions defined in the previous item can actually be achieved.

- The availability of positron polarisation is very important to achieve a small systematic uncertainty on the polarisation, since it introduces redundancy which overconstrains the system. Without positron polarisation, the uncertainties on A_{LR} from the global fit discussed in the previous item would be larger by a factor of 10.

3.2 Beam energy measurement

For each beam, energy spectrometers [20] will measure the beam energy before and after the collision point to a precision of $\delta E_b/E_b = 10^{-4}$. The upstream and downstream spectrometers are based on complementary approaches and have been designed to achieve the target precision over the full range of possible ILC beam energies from 45.6 to 500 GeV.

These measurements can be augmented by exploiting the collision data themselves. In particular, in $e^+e^- \to \mu^+\mu^-\gamma$ events, the transverse momenta and angles of the muons are precisely measured using the tracking system of the detectors. Then, from energy and momentum conservation, the center-of-mass energy of the collision can be extracted without the need to detect the photon. This method can reach statistical precisions of $\delta E_b/E_b = 10^{-5}$ or better at all center-of-mass energies. The dominant systematic uncertainty is the momentum scale of the detector [29].

The detector's momentum scale can be calibrated using the J/Ψ, whose mass is known to 1.9×10^{-6} [16]. Based on a run at the Z pole providing 10^9 hadronic Z events, the statistical uncertainty on the reconstructed mass peak position in di-muons will be smaller than 2×10^{-6} [30]. This means that the absolute momentum scale can be determined sufficiently well to match the requirements of the method described in the previous paragraph and produce an absolute $\delta E_b/E_b$ of 10^{-5}.

The point-to-point energy uncertainty, *e.g.*, during a resonance or threshold scan, will reach similar precisions. While the absolute energy scale does not affect the measurements of the point-to-point variations, the statistics of each data set during a scan will usually be smaller than in the main (peak) sample. Thus, the in-situ methods will typically be statistically limited: for a 10 times smaller sample, the statistical precision will be a factor 3 worse. On the other hand the beam energy spectrometer precision given above is by far dominated by the absolute calibration of

the beam position monitors. Relative changes in the beam position can be measured much more precisely. Therefore the combination of in-situ methods and the energy spectrometers will allow a determination of the energy of smaller data sets with precision equal to that of the absolute energy of a main data set.

3.3 Luminosity measurement

At all lepton colliders, the luminosity spectrum is broadened by initial-state radiation. At linear colliders (and high-luminosity circular colliders) there is additional radiation due to the beam-beam interaction ("beamstrahlung"). The exact shape of the distribution of the luminosity as a function of the event-by-event CM energy is called the luminosity spectrum. This spectrum has a peak near the nominal CM energy with spread given by the intrinsic energy spread of the beams, which is estimated to be 10^{-3} [13], and a long tail to lower CM energies due to beamstrahlung. The average energy loss in this tail is a few percent at ILC250 but becomes increasingly important at higher CM energies.

Beamstrahlung depends on the instantaneous machine parameters and thus must be directly measured. In the study [31] for CLIC at $\sqrt{s} = 3$ TeV, the luminosity spectrum was reconstructed from radiative Bhabha events bin-by-bin with a maximum error of 5% over the whole energy range, leading to a residual systematic effect on energy and mass observables of a few 10's of MeV. At the ILC, with much less beamstrahlung, the precision is expected to improve to the percent level. As for the polarisation and beam energy measurements, a long-term determination of the luminosity spectrum from physics events will be combined with fast extractions of beam parameters from the pattern of e^+e^- pairs and photons in the very forward calorimeters BeamCal and GamCal [32], which can be performed every few bunch crossings. An example of propagating the results from [32] to a full physics analysis can be found in [33]. In this example, the effect on signal and background predictions is found to be at the few per mille level even when only using the "online", BeamCal-based method and not the full Bhabha analysis.

The absolute luminosity above 80% of the nominal center-of-mass energy can be determined from low-angle Bhabha scattering measured in the dedicated forward calorimeters of the ILC detectors to a precision of a few per mille [34].

4 Precision W measurements at 250 GeV

Two of the main experimental observables of interest for precision tests of the SM in the W boson sector are the W mass, m_W, and the W width, Γ_W. The ILC program with polarised beams and all standard stages of the machine is well suited

σ_M (GeV)	Δm_W (MeV)	$\Delta\Gamma_W^a$ (MeV)	$\Delta\Gamma_W^b$ (MeV)
1.0	0.67	1.3	2.0
2.0	0.98	1.7	2.7
2.5	1.1	2.0	3.2
3.0	1.3	2.3	3.7
4.0	1.6	2.8	5.0

Table 3: Statistical uncertainties for m_W and Γ_W expected for a sample of 10^7 reconstructed W bosons at the ILC250. These are estimated from a simple parametric fit of the Breit-Wigner lineshape convolved with a range of constant Gaussian experimental mass resolutions, σ_M, ranging from 1 to 4 GeV. The m_W uncertainty is evaluated with a one parameter fit with the width and mass resolution fixed. The corresponding uncertainties on the W width are evaluated either with the mass resolution fixed and known perfectly from a two parameter fit (Γ_W^a), or more realistically, from a three parameter fit (Γ_W^b) that also fits for the mass resolution.

to such measurements, and especially at $\sqrt{s} = 250$ GeV where data can be collected synergistically with Higgs boson related studies.

4.1 Measurement of m_W

The W mass has been a prime target for the ILC and has been understood to be very tractable based on extrapolations of measurements from LEP2 both well above W-pair threshold, and at W-pair threshold. Prior prospects for such measurements are summarized in Tables 1-9 and 1-10 in [35].

Measurements from LEP2, the Tevatron, and ATLAS of m_W have led to today's precision in the PDG of 12 MeV, with the best single experiment measurement having a quoted precision of 18 MeV. Further improvements from long-existing hadron collider data sets at the Tevatron and LHC are possible, and it was suggested in [35] that the LHC could eventually improve the uncertainty on the W mass to 5 MeV. But, given the predominant systematic uncertainties, this goal now looks very challenging.

It is then interesting to study the challenges to a high-precision measurement of m_W at lepton colliders. Data sets at LEP2 totalled 0.7 fb^{-1} per experiment, leading to statistically limited measurements. The ILC250 is expected to produce a much larger data set of 2 ab^{-1}, with polarised beams. This data set will provide a sample of more than 10^7 reconstructed W bosons. To demonstrate the statistical power of such a sample, we show in Table 3 the expected statistical uncertainties on m_W and Γ_W that would result from fits to the measured W boson invariant mass distribution. For a typical mass resolution of 2.5 GeV, 10^7 W bosons would yield a statistical uncertainty on m_W of 1.1 MeV. Similarly, fitting the mass, width, and a Gaussian experimental mass resolution, the total width could be determined from the lineshape

with a statistical uncertainty of 3.2 MeV. Thus, the measurements of these quantities at the ILC250 will already reach the regime in which systematic errors dominate. We will discuss the expected systematic errors for each proposed method in the remainder of this section.

The W boson total width can also be determined by the measurement of the W leptonic branching fractions, since the absolute leptonic partial widths, including new physics contributions, can be predicted from precision electroweak observables. We will discuss the measurement of $BR(W \to \ell\nu)$ in Sec. 4.2.

There are a number of promising approaches to measure the W mass at an e^+e^- collider such as ILC. Given the data sets that represent more than three orders of magnitude increase in statistics beyond LEP2, it is appropriate to also consider W mass measurement methods that may have better systematic behavior in this high statistics regime. The various methods for m_W measurement are as follows:

1. **Constrained reconstruction.** Kinematically-constrained reconstruction of $\mathrm{W^+W^-}$ using constraints from *four-momentum conservation* and optionally mass-equality, as was done at LEP2.

2. **Hadronic mass.** Direct measurement of the *hadronic mass*. This can be applied particularly to single-W events decaying hadronically or to the hadronic system in semi-leptonic $\mathrm{W^+W^-}$ events. This method does not rely directly on knowledge of the beam energy or its distribution.

3. **Lepton endpoints.** The two-body decay of each W leads to endpoints in the lepton energy spectrum at

$$E_\ell = E_\mathrm{b}(1 \pm \beta)/2 \ , \tag{1}$$

   where β is the W velocity. These can be used to infer m_W. The endpoints correspond to leptons parallel and anti-parallel to the W flight direction This technique can be used for both semi-leptonic and fully-leptonic WW events with at least one prompt electron or muon.

4. **Di-lepton pseudo-mass.** In WW to dilepton events, with electrons or muons, one has six unknown quantities, namely, the three-momenta of each neutrino. Assuming four-momentum conservation and equality of the two W masses, one has five constraints. By assuming that both neutrinos are in the same plane as the charged leptons, the kinematics can be solved to yield two "pseudo-mass" solutions that are sensitive to the true W mass. This technique was discussed in Appendix B of [36] and used along with the lepton endpoints by the OPAL experiment at LEP2 [37].

5. **Polarised Threshold Scan.** Measurement of the W^+W^- cross-section near threshold with longitudinally polarised beams is discussed in [38] and references therein. The ability to "turn-on" and "turn-off" the signal with polarised beams, a capability unique to ILC, allows a precise in-situ measurement of the background.

Methods 1,2,3,4 can all exploit the standard ILC program at 250 GeV and above. Method 5 needs dedicated running near $\sqrt{s} = 161$ GeV. Methods for measuring the W mass in e^+e^- colliders were explored extensively in the LEP2 era, see [39, 40] and references therein.

For ILC-sized data sets, the constrained reconstruction approach (method 1) may need to be restricted to semi-leptonic events in order to avoid the final-state interaction issues that beset the fully hadronic channel. With the large data-sets of WW events expected above threshold, the expectation is that this measurement will be systematics limited. With much improved detectors compared to LEP2 and with much better lepton and jet energy resolution, it is expected that uncertainties in the few MeV level can be targeted. Table 1-9 in [35] estimates an uncertainty of 2.8 MeV at $\sqrt{s} = 250$ GeV based on extrapolating LEP2 methods using only the semi-leptonic channels with electrons or muons.

Method 2 is based purely on the hadronic mass and was not used explicitly at LEP2. With the increased cross-section for singly-resonant events ($e^+e^- \to \mathrm{We}\nu$) at higher $\sqrt{s}$, the excellent resolution for particles in jets expected from particle-flow detectors, and the availability of control channels with hadronic decays of the Z, an opportunity exists to make a competitive measurement also using this method. However the demands on the effective jet energy scale calibration are very challenging. It was estimated (Table 1-10 in [35]) that a m_W uncertainty of 3.7 MeV could be reached. This would be dominated by the hadronic energy scale systematic uncertainty.

The endpoints method 3 was only used for fully leptonic events at LEP2. It has the inherent advantage that the systematic uncertainties are dominated simply by the uncertainties on the lepton energy scale and the beam energy, given that one can express m_W in terms of the endpoints as follows:

$$m_W^2 = 4E_l(E_\mathrm{b} - E_l) \ . \tag{2}$$

It may be worth considering this as a complementary method also for semi-leptonic events, that is of course correlated with the constrained reconstruction method.

The pseudo-mass method and the endpoints method were applied to the fully leptonic channel in [37]. Very little correlation (+11%) was found between the two methods, indicating that the two methods can be independently effective and can be combined. The OPAL result achieved a statistical uncertainty of 390 MeV on m_W

using 0.7 fb^{-1} of data. The lepton energy resolution for ILC detectors is about 0.15% based on momentum measurements; this is much better than the 3% energy (for electrons) and 8% momentum (for muons) resolutions at OPAL. Assuming a factor of two improvement for ILC detectors, (note that resolutions much less than Γ_W are not necessary), and the statistics of the 2 ab^{-1} data set at ILC250. we project a statistical uncertainty on m_W of around 3.6 MeV. This looks very promising, since the experimental systematic uncertainties are very straightforward; more detailed studies should be pursued. With the standard 10 ppm uncertainty on center-of-mass energy and detector momentum scale, this approach promises to be very fruitful with the full ILC program.

Method 5 needs dedicated running near $\sqrt{s} = 161$ GeV. This is now feasible for the ILC machine. The expected integrated luminosity is about 125 fb^{-1}/year if the run is done after the Luminosity Upgrade in Fig. 1. The use of a threshold scan with polarised electron and positron beams to yield a precision measurement of m_W at ILC was studied in [38]. One of the potentially dominant systematic uncertainties, the background determination, is under very good experimental control because of the polarised beams. This is difficult to achieve with an unpolarised collider. Errors at the few MeV level can be envisaged. With 100 fb^{-1}, and polarisation values of (90%, 60%), the estimated uncertainty is

$$\Delta m_W(\text{MeV}) = 2.4\,(\text{stat}) \oplus 3.1\,(\text{syst}) \oplus 0.8\,(\sqrt{\text{s}}) \oplus \text{theory}\ , \tag{3}$$

with these values added in quadrature, amounting to an experimental uncertainty of 3.9 MeV. With standard ILC polarisation values of 80% and 30% the estimated precision is 6.1 MeV. Eventual experimental precision approaching 2 MeV from this approach can be considered at ILC if one is able to dedicate 500 fb^{-1} to such a measurement, and the physics perspective of the day demands it. There are excellent prospects for very competitive ILC measurements of the W mass from the four other methods using data collected above the production threshold for Higgs bosons, and so it would seem premature to make exclusive running at W-pair threshold a requirement for the ILC run plan. Nevertheless, given the complementary nature of a threshold-based measurement it would seem prudent to retain accelerator compatibility with such a scenario.

Given that the leading experimental systematic uncertainties for the different methods are reasonably complementary, it is expected that, with the combination of these five different methods, ILC will be able to measure m_W to at least 2.5 MeV. This uncertainty can potentially already be reached with data-taking at the ILC250.

4.2 Measurement of W branching fractions

With the large data sets envisaged at ILC250, one can also target much improved measurements of the WW production cross section and the individual W decay

branching fractions. This would use the ten different final state cross sections available from WW production: the six WW final states associated with fully leptonic final states with two charged leptons (dielectrons, dimuons, ditaus, electron-muon, electron-tau and muon-tau), the three semileptonic WW final states, one for each lepton flavor, and the fully hadronic WW final state. This follows the methodology used at LEP2 [41–44].

The ten measured event yields can be fitted for an overall WW cross section, σ_{WW}, and the three individual leptonic branching fractions, B_e, B_μ and B_τ with the overall constraint that

$$B_{\rm had} = 1 - B_e - B_\mu - B_\tau \ , \tag{4}$$

taking into account background contributions in each channel. With ten channels and four fit parameters, there is some redundancy in the fitting procedure. This means that the parameters can be determined well even if the more challenging channels, namely the fully hadronic, the semileptonic with a tau, and the di-tau channel would end up being systematically limited. At LEP2, the signal process was modelled simply through the three dominant, doubly resonant Feynman diagrams (so called CC03 process), while other diagrams and their interferences resulting in the same four fermion final state, such as those for ZZ or $We\nu$, were treated as background. These "4f-CC03" corrections were typically about 10% depending on final state. A complete calculation of $e^+e^- \to 4f$ final states would need to be used in the high statistics regime.

We have looked into the feasibility of this method for ILC250, building on LEP2 studies at $\sqrt{s} \approx 200$ GeV, by putting together a fit ansatz that assumes identical efficiencies and mis-classification probabilities for all ten WW channels [44]. For the purpose of making an estimate for this report, we concentrate on the impact of a single subsample of the data. The actual analysis at the ILC will be based on global fit to the results from all polarisation modes, along the lines described in Sec. 3.

Of the total 2 ab^{-1} to be collected at ILC250, 0.9 ab^{-1} is to be collected with $e^-_L e^+_R$ enhanced collisions. These benefit from a WW cross section enhancement over unpolarised beams of a factor of 2.32 for $-80\%, +30\%$ beam polarisations. The estimated background per selection channel depends on the polarisation asymmetry of the different backgrounds and is estimated to be about +29% for the important two-fermion background from hadronic events. Taking this effect that leads to an increased background, and the decreased background estimated from $1/s$ scaling, we find that the unchanged OPAL background estimate is a good first estimate, and believe that this is a reasonably conservative estimate. We have based our estimates of statistical errors on the size of this subsample. We assume that the other 55% of the data set with the less favorable beam polarisation configurations is used to measure and test the background modeling and have neglected it for now in estimating statistical sensitivity.

We also include the 6% reduction in unpolarised cross section at $\sqrt{s} = 250$ GeV. Given that ILC detectors will have much improved forward hermeticity, jet and lepton energy resolutions, vertexing, and electron, muon, and tau identification, it is very reasonable to expect that the efficiency and background performance would be much better. One effect that is more difficult at higher $\sqrt{s}$ is a more forward polar angle distribution of the W decay products. We find that 94.7% of leptons in semi-leptonic events have a polar angle satisfying, $|\cos\theta| < 0.975$, whereas at $\sqrt{s} = 200$ GeV, the corresponding fraction is 96.7%.

It is straightforward to estimate statistical uncertainties and we have done so for a number of scenarios. For systematic uncertainties, there are five that come to mind:

- absolute integrated luminosity: The precision is likely limited to about 0.1%; however, to a great extent, this value cancels out of the determination of branching ratios.
- lepton efficiencies: This can be measured with high precision using control samples of di-leptons as was done for precise Z lineshape measurements preferably using a tag-and-probe method. The key element is efficiency within the geometrical acceptance. With control samples totalling 10^7 leptons, statistical uncertainties of 3×10^{-5} can be targeted assuming highly efficient lepton identification.
- hadronic system modeling: Uncertainties of order 0.03% seem feasible based on LEP1 hadronic Z studies targeted at estimating the hadronic efficiency/acceptance.
- fake τ candidates from hadronic events: One needs to be able to model the rate of isolated tracks from hadronic systems that can fake tau candidates. This should be easier to reduce than at LEP2 given the excellent vertexing performance envisaged.
- background estimation: This will be controlled with the less signal-favorable beam polarisation configurations.

In Table 4 we show the expected absolute statistical uncertainties for two different parameterizations, one based on the three leptonic branching fractions, (B_e, B_μ and B_τ) and one based on B_e and the ratios B_μ/B_e and B_τ/B_e. Five different configurations of included event selections are considered, indicating a reasonable degree of robustness. The fits also fit for the cross section but the absolute value is likely to be systematics limited. It can be seen that fractional statistical uncertainties on B_e below 0.1% and as low as 0.04% can be envisaged. The fits do not assume lepton universality. The data set considered consists of 29.7 million WW candidates. The efficiency systematics seem not to be limiting. The main systematic issue is likely to be the background estimation that should be facilitated with the various polarised

Event selections	B_e	B_μ	B_τ	R_μ	R_τ
All 10	4.2	4.1	5.2	6.1	7.5
9 (not fully-hadronic)	5.9	5.7	6.4	6.1	7.5
9 (not tau-semileptonic)	4.6	4.6	7.8	6.1	10.8
8 (not f-h and not τ-semileptonic)	8.3	8.4	7.8	6.1	12.8
7 (not f-h and not τ-sl and not di-τ)	9.0	9.1	10.6	6.1	16.7

Table 4: Statistical uncertainties, expressed as relative errors in units of 10^{-4} for the leptonic branching fractions of the W boson (B_e, B_μ and B_τ) and the ratios of branching fractions $R_\mu = B_\mu/B_e$, $R_\tau = B_\tau/B_e$. The lines of the table refer to different choices of the included event selections. The values assume ILC measurements at $\sqrt{s} = 250$ GeV using the 45% of the 2 ab^{-1} integrated luminosity with enhanced $e^-_L e^+_R$ collisions, with the same efficiencies and the same background cross sections as in the OPAL measurement [44]. The uncertainties given for R_μ, R_τ are from a separate fit using the (B_e, R_μ and R_τ) parametrization.

data sets. The event selection purity will likely need to be tightened to reduce systematics from backgrounds, but the current statistical estimates should be a reasonable starting point.

5 Precision electroweak observables

Electroweak precision observables measured at LEP and SLC at the Z pole continue to provide the backbone of the interpretation of measurements in the electroweak sector. A comprehensive overview of these measurements is given in [17]. In the next few sections, we will explain how the ILC will improve on these measurements.

To set up the discussion to follow, we now define the basic precision observables. For simplicity, we express the observables here in terms of tree-level formulae and describe each observable as having an independent measurement. In practice, the values of observables and the beam properties will be combined in a global fit, as described in the third bullet of Sec. 3.1.

For a given quark or lepton flavor f, let g_{Lf}, g_{Rf} be the helicity-dependent Zff couplings. Then the quantities, for quarks q,

$$R_q = \frac{\Gamma(Z \to q\bar{q})}{\Gamma(Z \to \text{hadrons})} \ , \tag{5}$$

and, for leptons $\ell = e, \mu, \tau$,

$$1/R_\ell = \frac{\Gamma(Z \to \ell^+\ell^-)}{\Gamma(Z \to \text{hadrons})} \ , \tag{6}$$

are given, at the tree level, by

$$R_q \ , \ 1/R_\ell \propto (g_{Lf}^2 + g_{Rf}^2) \ , \tag{7}$$

and the Z decay polarisation asymmetries are given by

$$A_f = \frac{g_{Lf}^2 - g_{Rf}^2}{g_{Lf}^2 + g_{Rf}^2} \ . \tag{8}$$

It is useful to define the value of $\sin^2\theta_w$ governing the Z couplings from the electron asymmetry as "$\sin^2\theta_{eff}$" given by the formula

$$A_e = \frac{(\frac{1}{2} - \sin^2\theta_{eff})^2 - (\sin^2\theta_{eff})^2}{(\frac{1}{2} - \sin^2\theta_{eff})^2 + (\sin^2\theta_{eff})^2} \approx 8(\frac{1}{4} - \sin^2\theta_{eff}) \ . \tag{9}$$

It is this value of $\sin^2\theta_w$ that enters the Zh and WW pair production cross sections that are most important in determining the Higgs boson couplings.

Loop corrections to the SM predictions for Z observables given in terms of $\sin^2\theta_{eff}$ are at the parts per mille level. Thus, it is accurate to quote projections for the precision of future experiments from tree-level formulae involving $\sin^2\theta_{eff}$. Of course, actually extracting Z couplings from cross section measurements at the 10^{-4} level of precision requires that the SM contributions to these cross sections be known to comparable accuracy. The nontrivial requirements for theory are reviewed in [45].

Often, the leptonic asymmetries A_e, A_μ, and A_τ are combined to give a composite leptonic asymmetry. Here, we will distinguish these three quantities and discuss tests of models that allow small differences in the Z couplings to e, μ, and τ.

At a polarised e^+e^- collider, A_e is given by the left-right asymmetry in the total rate for Z production,

$$A_e = A_{LR} \equiv \frac{\sigma_L - \sigma_R}{(\sigma_L + \sigma_R)} \ , \tag{10}$$

where σ_L and σ_R are the cross section for 100% polarised $e_L^- e_R^+$ and $e_R^- e_L^+$ initial states. For beams not perfectly polarised, the effective left-handed polarisation of the initial state is given by

$$P_{eff} = (P_{e^-} - P_{e^+})/(1 - P_{e^-}P_{e^+}) \ , \tag{11}$$

and the measured asymmetry is proportional to P_{eff}. The determination of the quantity A_e then requires only an excellent knowledge of the polarisation and knowledge that the acceptance in the decay modes studied does not change when the polarisation is flipped. Essentially, the entire statistics of Z production can contribute to the measurement. We find that the dominant systematic error is that on the value of the polarisation. We have discussed how this systematic is controlled in Sec. 3.1.

For other asymmetries, beam polarisation can also play a role. These quantities are measured from the left-right forward-backward asymmetry

$$A^f_{FB,LR} \equiv \frac{(\sigma_F - \sigma_B)_L - (\sigma_F - \sigma_B)_R}{(\sigma_F + \sigma_B)_L + (\sigma_F + \sigma_B)_R} \ , \tag{12}$$

where, again, L and R refer to states of 100% polarisation. At the tree level,

$$A^f_{FB,LR} = \frac{3}{4} A_f \ . \tag{13}$$

At an unpolarised collider, the values of the A_f are obtained from quantities such as the unpolarised forward-backward asymmetries,

$$A^f_{FB} \equiv \frac{(\sigma_F - \sigma_B)}{(\sigma_F + \sigma_B)} \ . \tag{14}$$

At the tree level,

$$A^f_{FB} = \frac{3}{4} A_e A_f \ , \tag{15}$$

so there is some sacrifice of statistics to achieve the same level of precision. (The determination of A_τ is a special case, to be discussed below.) For some purposes, for example, to test lepton universality, we wish to know the ratio of A_f to the precisely determined value of A_e. In such ratios of polarisation asymmetries measured in the same run, the systematic uncertainty on the polarisation cancels out.

The uncertainties from acceptance and particle identification largely cancel out of the A_f measurements, but in the measurements of R_f they are the major source of systematic error. In the LEP experiments, the measurements of the rates of Z decay to $b\bar{b}$ and $c\bar{c}$ were mainly done with single-tag methods that required a "dilution factor" correction with a large QCD uncertainty. At the ILC, the efficiencies for b and c identification and also the statistics to determine these efficiences precisely, will be much higher. The absolute tagging efficiences can be measured from $e^+e^- \to f\overline{f}$ events, using a probe and tag method. We assume an uncertainty of 0.1% in the efficiency for b tagging and an uncertainty of 0.5% in the uncertainty for charm tagging. These values are based on an extrapolation of the results of $e^+e^- \to ZZ$ studies described in [46]. It would be valuable to confirm these values with a full-simulation study at the higher statistics required here, and that analysis is in progress. Note that, while these values affect our projections for the precision electroweak uncertainties given in Table 9, they do not significantly affect the uncertainties on Higgs boson couplings quoted in Table 10.

For asymmetry measurements, we must also discriminate f from $\overline{f}$. There is a correction due to sign flips, which must be estimated. This can be done using vertex, lepton, or kaon charges, collecting a sample of events with non-contradictory charges $(-+, +-)$. To understand the effect of sign flips, we can use also the sample of events

with like charges ($--$, $++$). This allows us to determine from the data themselves the fraction of correctly reconstructed events and the fraction of events that have suffered from migrations. Thus, there is no need to calculate a dilution factor from first principles and there is no systematic error associated with dilution. There is only a statistical error that can be combined with other sources of statistical error.

6 Precision electroweak at 250 GeV from radiative return

In this report, we will discuss two methods by which the ILC will improve on the precision measurements of the Z properties and couplings. The highest precision measurements will come from a GigaZ run, described in Sec. 2.2. We will present a detailed discussion of the GigaZ capabilities in Sec. 7.

However, we should not overlook the fact that the ILC running at 250 GeV will already produce a data set that will allow substantial improvements of our knowledge of precision electroweak observables. One of the high-cross-section reactions at 250 GeV is the radiative return to the Z, $e^+e^- \to Z\gamma$. In this reaction, the Z is produced in the forward direction but still accessible to the ILC detectors. We will explain in a moment that the photon, which is produced in the opposite forward direction, does not need to be observed to provide a very clean event sample. The ILC program, with 2 ab^{-1} of data, will produce roughly 77 million hadronic Zs and 12 million leptonic Zs, a substantial increase over the event sample of LEP. Further, these events are produced with polarised beams, so that, for polarisation observables, the event sample to compare with is that of SLC. The full power of the ILC detectors can be used for flavor identification.

We tag the signal events for the radiative return analysis based on the polar angles of the two fermions from $Z \to f\overline{f}$. To describe the method simply, we will use the approximations that the fermions are massless and the photon is collinear to the beam directions. This is already quite close to realistic, and the approximations can be relaxed with small corrections. Then let E_i and θ_i, $i = 1, 2$, denote the energy and polar angle, respectively, of each final lepton or jet. Transverse momentum conservation implies that $E_1 \sin\theta_1 = E_2 \sin\theta_2$. The fermion pair is boosted only in the beam direction. The boost factor can be determined as

$$|\beta| = \frac{|E_1 \cos\theta_1 + E_2 \cos\theta_2|}{E_1 + E_2} = \frac{|\sin(\theta_1 + \theta_2)|}{\sin\theta_1 + \sin\theta_2}. \tag{16}$$

It is interesting that the E_i cancel out, so β only depends on θ_1 and θ_2. The invariant mass of the fermion pair, m_{12}, can then be reconstructed as

$$m_{12}^2 = \frac{1 - |\beta|}{1 + |\beta|} \cdot s \ , \tag{17}$$

where $\sqrt{s}$ is the center-of-mass energy. For the signal events we expect that m_{12} peaks at m_Z and, for $\sqrt{s} = 250$ GeV, $|\beta|$ peaks at 0.76. The angles θ_1 and θ_2 can be measured very precisely at the ILC detectors, so that the signal events can be tagged without the need to observe the ISR photon.

This method was actually used at LEP2 [47], though mainly for calibrating the beam energy due to the limited statistics. But at ILC250, we will expect 90 million of such radiative events, a factor of 5 (100) more than the total number of Z produced at LEP (SLC).

A fast simulation study has been performed for the A_e measurement using the $e^+e^- \to \gamma Z$, $Z \to q\bar{q}$ channels and the full SM background [48]. After all the selection cuts, the signal efficiency is 73% and the remaining background events, due to systems with approximately the Z mass from other processes, are almost negligible, as shown in Fig. 2. For the results shown, realistic effects from finite fermion mass and beam crossing angles have already been taken into account. The events in which the photon goes into the detector have not been separated, but it should be straightforward to do, provided that they only contribute as a small fraction of total events. From the measured cross sections for the left- and right-handed beam polarisations, A_e can be determined from Eq. (10). The statistical error on A_e for 2 ab^{-1} data in the ILC250 scenario is estimated to be 0.00015. We can perform the same analysis using the $Z \to l^+l^-$ channels. The combined statistical error is expected to be $\Delta A_e = 0.00014$, a relative error of $\delta A_e = 9.5 \times 10^{-4}$. This is a factor of 10 improvement over the current uncertainty on A_e. Many systematic errors in the cross section measurement cancel out in the measurement of this asymmetry. The dominant systematic error for A_e will come from the uncertainty in P_{eff}. In Sec. 3.1, we have explained that, through the measurement of processes with large polarisation asymmetries such as $e^+e^- \to WW$, the relative systematic error on A_e can be reduced to 3×10^{-4}.

In principle, the value of A_e also depends on the CM energy in the $e^+e^- \to Z\gamma$ reaction. The polarisation asymmetry actually measured in this reaction has the form [49]

$$A_{obs} = A_e + \Delta A, \tag{18}$$

where ΔA is a correction due to interference between the contributions to the $e^+e^- \to f\bar{f}\gamma$ from the resonant diagram with an intermediate Z and the nonresonant diagram with an intermediate γ. At the Z pole, the interference term has significant energy-dependence, requiring excellent knowledge of the CM energy. This will be an issue in Sec. 7.1. However, for the radiative return process at 250 GeV, the dependence $\Delta A_e/\Delta E_{CM}$ is 3 orders of magnitude smaller, allowing us to safely ignore the systematic error from the beam energy uncertainty.

For A_f measurements other than A_e, we need to measure the left-right forward-backward asymmetry defined in Eq. 12. A dedicated simulation study for A_f ($f = b/c/\mu/\tau$) has not yet been performed. Nevertheless we can estimate the signal effi-

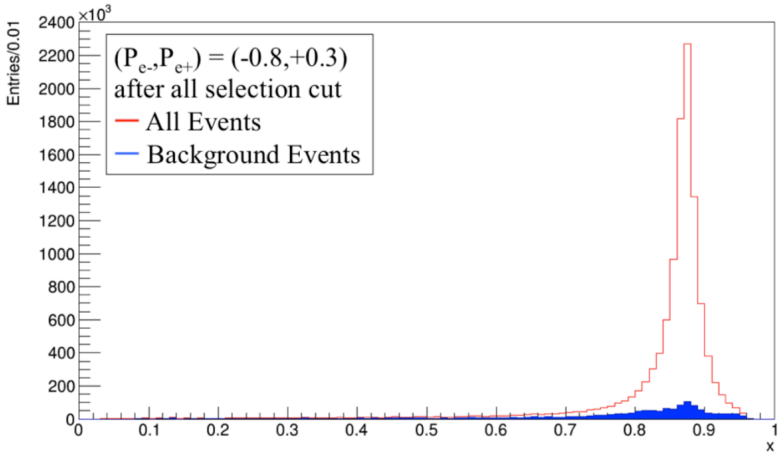

Figure 2: Reconstructed distribution of $x \equiv \frac{2|\beta|}{1+|\beta|}$ for the signal $e^+e^- \to \gamma Z$, $Z \to q\overline{q}$ and from background events that mimic this signal, at $\sqrt{s} = 250$ GeV with an integrated luminosity of 250 fb^{-1}.

ciency in two steps based on existing simulation analyses. The first step is to tag the signal events as from radiative return, just as in the A_e measurement. The second step is to identify the flavor and charge of the fermion. For example, the efficiency for the A_b measurement can be estimated to be 73% × 40% in which the 73%, for tagging the hadronic radiative return event, is from fast simulation analysis described above [48], and the 40%, for b-tagging and b charge identification, is from a full simulation analysis described in [50]. The statistical error of A_b is then estimated to be $\Delta A_b = 0.00053$, a relative uncertainty of $\delta A_b = 5.7 \times 10^{-4}$. Similarly, the efficiencies for A_c, A_τ and A_μ can be derived from full simulation results in [51–53]. These are estimated to be 73% × 10%, 80%, and 88%, respectively. Their statistical errors are summarized in Table 9. The dominant systematic error is expected to come from the uncertainty in the effective beam polarisation P_{eff}.

The measurements of $R_f(1/R_f) \equiv \Gamma(Z \to f\overline{f})/\Gamma(Z \to \text{hadrons})$, for $f = b/c$ ($f = e/\mu/\tau$), are simpler to describe, since we only need to measure the total rate for each flavor without the need to identify the charge. The signal efficiencies can be estimated based on the same analyses cited above [48,50–53]. The expected statistical errors are summarized in Table 9. The dominant systematic errors would come from the uncertainties in the flavor-tagging efficiencies, estimated in Sec. 5 to be 0.1% for $f = e/\mu/\tau/b$ and 0.5% for $f = c$.

Noting that R_e is expected to be improved by a factor of 2 over the current uncertainty [16], it is interesting to convert this to a value of the quantity $\Gamma_e \equiv \Gamma(Z \to e^+e^-)$, which is a useful input to the SMEFT global fit for Higgs boson couplings that will be discussed in Sec. 10. Γ_e can be derived from the measurements

of the cross section of Z to hadrons $\sigma_{\rm had}$, the Z total width Γ_Z, and R_e, with the uncertainty estimated as

$$\delta\Gamma_e = \frac{1}{2}\delta\sigma_{\rm had} \oplus \frac{1}{2}\delta\Gamma_Z \oplus \frac{1}{2}\delta R_e \ , \tag{19}$$

where δ denotes a relative uncertainty: $\delta A = \Delta A/A$. With the current uncertainties for $\sigma_{\rm had}$ and Γ_Z from [16], and expected uncertainty for R_e at ILC250, we expect the precision for Γ_e to decrease to $\delta\Gamma_e = 0.86 \times 10^{-3}$. This improves over the current relative uncertainty on $\Gamma(Z \to \ell^+\ell^-)$ of 1.02×10^{-3} and also allows us to relax the assumption of lepton universality in this input to the SMEFT fit.

7 Precision electroweak from the GigaZ program

A further imprement of precision electroweak observables is possible in the GigaZ program described in Sec. 7. As shown in Table 2, the GigaZ program will produce about 5×10^9 Z events. This is equivalent to about 250 times more than has been collected at LEP by all four experiments, thus promising improvements of electroweak observables by more than one order of magnitude. The machine would be operated with polarised beams with a degree of polarisation of |80%| for electrons and |30%| for positrons.

7.1 Measurements of the weak mixing angle

We first discuss measurements of the effective weak mixing angle $\sin^2\theta_{eff}$, defined in Eq. 9, and, more general, the leptonic left-right asymmetries A_ℓ for $\ell = e, \mu, \tau$. At a linear collider with polarised beams the effective weak mixing angle can be extracted in several ways but notably by measuring the left-right asymmetry A_{LR}, Eq. (10). Using this method, SLD achieved the highest-precision single measurements of $\sin^2\theta_w$, even though LEP had collected about 30 times more luminosity.

At GigaZ, using all hadronic decay modes of the Z, the statistical error on A_{LR} will be a few times 10^{-5}. The measurement will then be dominated by the systematic error on the polarisation. As we have explained in Sec. 3.1, we expect a systematic error on the beam polarisation of 0.05% for a realistic assumption of 0.25% of the precision of the polarimeters. Positron polarisation plays a crucial role in reaching this low level of uncertainty.

A precise measurement of A_{LR} at the Z pole requires also excellent control over the value of the beam energy. The observed polarisation asymmetry has a strong energy-dependence due to the interference of the s-channel Z and γ diagrams: $dA_{LR}/dE_{CM} \approx 2 \times 10^{-5}/\text{MeV}$. But we have argued in Sec. 3.2 that the beam energy in GigaZ can be

measured, by a combination of methods, to a precision of 1 MeV. This is of similar size to the statistical error. We note that this A_{LR} measurement is specifically a measurement of A_e.

The values of A_μ and A_τ can also be improved at GigaZ by measuring the corresponding left-right forward-backward asymmetries, Eq. (10). Note that, for a lepton species, the left-right forward-backward asymmetry at the Z is 7 times larger than that unpolarised forward-backward asymmetry and less subject to radiative corrections. It is interesting to test lepton universality by comparing these quantities to the precisely measured value of A_e. The systematic error due to the polarisation cancels out in the ratios, so A_μ and A_τ can be compared to A_e with a relative uncertainty of about 0.02%.

The higher statistics available from GigaZ will of course improve the measurements of R_ℓ for each lepton species. The systematic errors are small. Also, these are due to knowledge of the acceptance, so it can be assumed that these errors scale with luminosity. To obtain the estimates in Table 9, we have simply rescaled the LEP results given in [17].

The absolute precision on $\sin^2\theta_{eff}$ of $1.3 \cdot 10^{-5}$ expected from GigaZ is nearly one order of magnitude better than the precision of the present world average $\sin^2\theta_w$ [16] and only a factor three worse than that claimed for FCCee [56]. This is reminiscent of the LEP/SLC scenario. It is worth recalling some details of the measurement of A_e at circular colliders. The best method is to use a wonderful formula from LEP: the τ polarisation at the Z varies with the τ production angle θ according to [57]

$$P_\tau(\cos\theta) = -\frac{A_\tau(1+\cos^2\theta) + 2A_e\cos\theta}{(1+\cos^2\theta) + \frac{8}{3}A_{FB}^\tau\cos\theta} \approx A_\tau + \frac{2\cos\theta}{(1+\cos^2\theta)}A_e \ . \qquad (20)$$

Since A_e controls the $\cos\theta$ asymmetry in this formula, it is in practice somewhat better determined than A_τ. This gives the best determination of $\sin^2\theta_{eff}$. The dominant systematic error in this technique is the uncertainty in the conversion of the measured energies of τ decay products to the underlying τ polarisation. This is complicated by the fact that all τ decay modes receive feed-down from other modes for which the observed energy spectrum of the visible decay products has a different dependence on the τ polarisation. In the LEP era, this cross-contamination was about 10% in each mode, but the modelling of τ decays was understood well enough to constrain this error on A_τ, A_e to be less than 1% (relative error). For FCCee, this understanding must be improved by two orders of magnitude. Some difficulties in achieving this are explained in [58].

7.2 Measurements of heavy quark production

Other important observables of the Z pole experiments are the Z couplings to the heavy quarks b and c. In this section, we discuss the measurement of these quantities

and some physics implications of those measurements. This subject is treated more comprehensively in [59]. Note, though, that [59] supposes an unpolarised positron beam.

We first present estimates of the precision of the determinations of R_b and R_c and of A_b and A_c. The basic methods for these measures were described in outline in Sec. 5. For the b observables, the efficiencies that determine the statistical errors are derived from the study of $e^+e^- \to b\bar{b}$ presented in [63]. For c, the statistical errors are extrapolations of those presented in [17].

The systematic errors bring in some more subtle points. Thanks to the excellent vertex detector and the small beam size, the ILC experiments are much closer to the SLD detector than the LEP detectors, and so one might take the SLD heavy quark analyses as a starting point. The relevant references for this are [60] and [61]. One finds that, apart from Monte Carlo statistics, there is not a single dominant source of systematic error. Instead, the total systematic error is composed of a number of small contributions. It is safe to assume that most of these contributions will be controlled to a sufficient level at the time of GigaZ, either by improved understanding of QCD or by higher-statistics measurements of $e^+e^- \to q\overline{q}$ processes. As an example, one large source of systematic error for c quark observables is the uncertainty from gluon splitting to a $c\bar{c}$ pair. Consulting the OPAL analysis in [62], one finds that the uncertainty of the splitting fraction was limited by statistics that did not allow for a sufficient reduction of the background from b-quark pairs. At GigaZ, it will be possible to take advantage of the much higher statistics in $q\overline{q}$ production both at GigaZ and at ILC250, and also the detector will be superior to the OPAL detector. It is therefore justified to assume that the gluon splitting can be controlled to a much better level than it was possible for OPAL. Since the measurements not statistics-limited, we can study the influence of other QCD effects by comparing to a fiducial region in which the heavy quark jets are approximately back-to-back.

Following these considerations, the dominant error source for A_b is given by the uncertainty of beam polarisation. In case of A_c we assume that the error of sources other than beam polarisation will roughly equal the error of beam polarisation. In case of R_b, the general improvement of the measurements justifies an improvement of the systematic error by a factor of five. (This improvement was already found in the studies for the TESLA Technical Design Report [55]). For R_c, it is justified to assume that the component of the systematic error that does not improve with statistics will be improved from SLC by a factor of about two.

We have already pointed out in Sec. 5 that the method for determining heavy quark forward-backward asymmetries will be much improved from that of LEP using the large sample of double-tagged events. The systematic error from this source in the LEP experiments will become a statistical error that is continuously improvable.

Figure 3 summarises the precisions expected at GigaZ for the heavy quark ob-

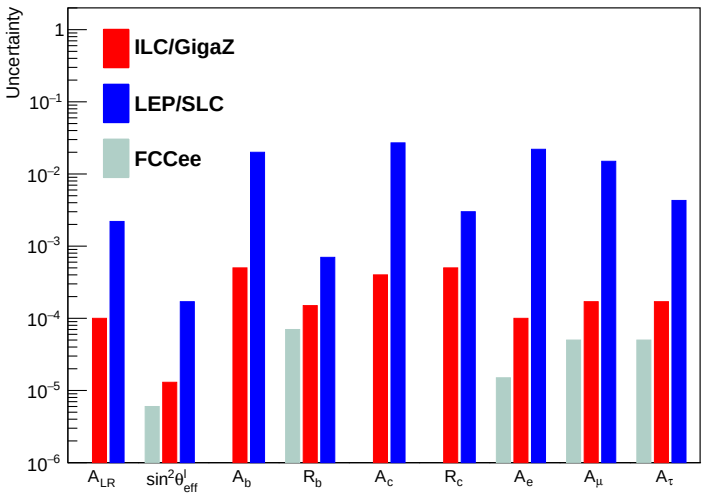

Figure 3: *Summary of the precision achievable at GigaZ compared with LEP/SLC results [17] and FCCee projections [56] for observables and derived quantities that are described in the text.*

servables. These results are also presented in Table 9 in Appendix A.

There are two important physics motivations for studying the heavy quark couplings to the Z beyond the general idea of finding higher-precision tests of the SM. The first is that the largest deviation of the precision electroweak observables from the SM predictions observed in the LEP/SLC program involves the b system. Assuming, following the SM expectation, that A_b is close to 1, one can extract A_e from a measurement of the b forward-backward asymmetry, using Eq. (14). At LEP, this determination gave results that differ from the arguably more direct measurements of A_e from the left-right asymmetry and the τ polarisation asymmetry by about 3.5 standard deviations. Actually, there is a lack of rapport that involves the three quantities A^b_{FB}, R_b, and A_e that frustrates theoretical explanations [64]. This issue calls for a new set of experimental measurements.

The second is the real possibility that the Z couplings to the b quark are altered by new physics. The b_L is in the same electroweak multiplet as the t_L, so if the top quark acquires its large mass from strong dynamics in the Higgs sector, the b_L also must feel the effects of this new strong sector. The direct coupling of the b to the Higgs sector can be made small since $m_b \ll m_t$, and the couplings of the b to photons and gluons are restricted by Ward identities, so the one place where such corrections are allowed to show up is in the b coupling to weak-interaction bosons. The b quark can also couple preferentially to Z' bosons associated with the Higgs strong interactions. All of these features are explicitly realized in Randall-Sundrum

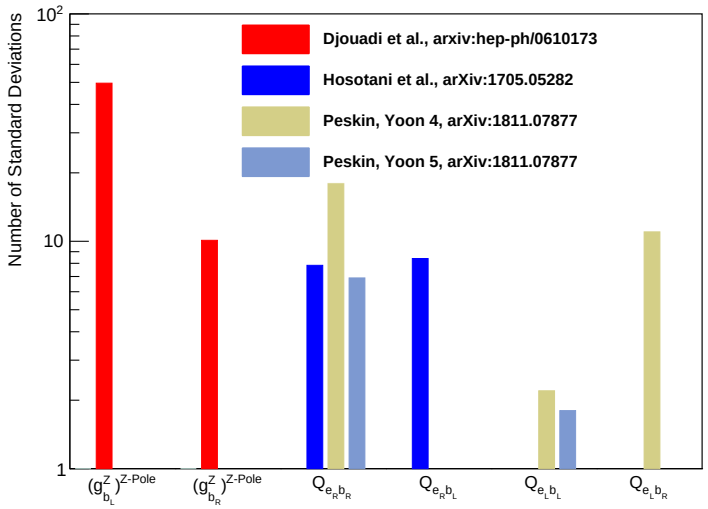

Figure 4: Visibility of deviations from the SM predictions in $g^Z_{b_j}$ and the helicity amplitudes $Q_{e_ib_j}$, in standard deviations, from combined ILC250/GigaZ running, expected from new physis models with Randall-Sundrum extra dimensions [65–67].

extra-dimensional models of the Higgs sector [65–67].

These expectations can be tested through measurements of $e^+e^- \to b\bar{b}$. For some models, the effects are already large enough to see at ILC250. Using polarisation and the forward-backward asymmetry, the ILC250 can measure the four helicity amplitudes associated with b couplings to Z and Z',

$$Q_{e_ib_j} = Q^\gamma_e Q^\gamma_f + \frac{g^Z_{e_i} g^Z_{b_j}}{s - m^2_Z} + \frac{g^{Z'}_{e_i} g^{Z'}_{b_j}}{s - m^2_{Z'}} \ . \tag{21}$$

for $i, j = L, R$. The second term can include effects of Z-Z' mixing [65]. For example, at ILC250, the quantity $Q_{e_Lb_R}$, which has a SM value of about 0.45, can be measured with a precision of $\Delta Q_{e_Lb_R} = 5 \times 10^{-4}$. If there is a deviation from the SM, we will want to resolve whether it comes from the Z couplings or the couplings to higher resonances. That could be done with a second measurement at the Z pole. To match the ILC250 determination, the Z pole measurment should reach a precision of 0.5%, achievable at GigaZ but a factor of 10 beyond the current precision from LEP. The sensitivity of models to combined ILC250/GigaZ running is shown in Fig. 4. The model of [66] predicts similar perturbation of the helicity amplitudes for the light fermions, so it is interesting to pursue these measurements also for the lighter flavors.

7.3 Measurements of total and partial widths

Using the improved knowledge of the beam energy discussed in Sec. 3.2, it will be possible to improve the systematic error on the width of the Z to about 1 MeV, with negligible statistical error [55]. This would be an improvement over the LEP uncertainty by more than a factor of 2. Given this improvement and the GigaZ improvement in R_e, the relative uncertainty in the quantity $\Gamma(Z \to e^+e^-)$ highlighted at the end of Sec. 6 improves to 0.56×10^{-3}.

In all, we see that the GigaZ program is surprisingly powerful. It has the capability to improve all of the R_f snd A_f precision observables by a factor of 10 from their current LEP and SLC values. In some cases, we obtain a much larger improvement. The program strongly benefits from the use of polarised beams and the high level of control that these give us over the limiting systematic errors. The full set of projected uncertainties for the GigaZ program is given in Table 9.

8 4-fermion processes

In addition to precision tests of the SM in Z boson couplings, the ILC will bring new tests of the SM in four-fermion interactions, which will be measured with precision at 250 GeV and higher energies. Within the SM, fermion pair production cross sections are very well understood and computed to part per mille accuracy. Precision measurements of these processes at e^+e^- colliders can recognize small deviations from these predictions. In this way, it is possible to test both for the presence of new s-channel electroweak resonances and for four-fermion contact interactions that represent the low-energy effective description of new electroweak sectors.

Several features of e^+e^- collisions make this type of search especially powerful. First, one knows that the initial state is e^+e^-, and it is possible to distinguish flavors in the final state. Also, in the approximation of ignoring initial- and final-state masses, the differential cross sections for 100% polarised $e^-_L e^+_R$ and $e^+_L e^-_R$ beams take the form

$$\begin{aligned}
\frac{d\sigma}{d\cos\theta}(e^-_L e^+_R \to f\overline{f}) &= \Sigma_{LL}(s)\ (1+\cos\theta)^2 + \Sigma_{LR}(s)(1-\cos\theta)^2 \\
\frac{d\sigma}{d\cos\theta}(e^-_R e^+_L \to f\overline{f}) &= \Sigma_{RL}(s)\ (1-\cos\theta)^2 + \Sigma_{RR}(s)(1+\cos\theta)^2
\end{aligned} \tag{22}$$

where Σ_{LL}, Σ_{RL} refer to $f_L\overline{f}_R$ production and Σ_{LR}, Σ_{RR} refer to $f_R\overline{f}_L$ production. This means that, with polarised beams, each process gives 4 independently measurable coefficients that can provide tests of the SM.

This section will discuss "universal" parameters of four-fermion interactions and parametrizations appropriate to production of light flavors. Pair-production of b and

t quarks within the SMEFT brings in a large number of operator coefficients; fits to this larger set of parameters are reviewed in Sec. 9.

8.1 Searches for Z' bosons

We first discuss the search for new s-channel Z' resonances. In Table 5, we present exclusion and discovery limits for various types of Z' bosons that are considered in the literature. A commonly used metric is the reach for the Sequential Standard Model (SSM) Z' whose couplings are assumed to be identical to the couplings of the Z boson of the SM. Another benchmark is the ALR model, which features a boson that couples to the right-handed $SU(2)$ acting on SM fermions with the same strength as the weak-interaction left-handed $SU(2)$. An actual Z' would have couplings orthogonal to the couplings of the Z, so actually, both the SSM and the ALR models are straw men. With this in mind, we also quote results for Z' bosons found in E_6 grand unified theories that extend the SM, canonically taken as the linear combinations ψ, χ and η of two bosons from the center of E_6 orthogonal to the SM directions. The limits in the table are based on an analysis of $e^+e \to f\overline{f}$, $f = e/\mu/\tau/b/c$, at 250 GeV using the ILD detector model and the full simulation framework described in Sec. 6 and 7 of [8], assuming a data set of 2 ab^{-1}. This analysis is described in some detail in [53]; we also include information from the studies in [50–52]. The background events in all of those channels are essentially negligible. The signal efficiencies in e, μ and τ channels are rather high, respectively 97%, 98% and 90%. For b and c channels, mainly due to charge identification, the efficiencies are much lower, 29% and 7%, respectively. The exclusion and discovery limits for Z' are obtained based on a χ^2 fit to the measured differential cross sections $\mathrm{d}\sigma/\mathrm{d}\cos\theta$ where θ is the polar angle of the fermion. Systematic errors are taken into account in the fit; they are assumed to 0.1%, 0.1%, 0.2%, 0.2% and 0.5% respectively for $e/\mu/\tau/b/c$ channels. We have extrapolated these results to ILC500 with 4 ab^{-1} and to ILC1000 with 8 ab^{-1}. The results for higher CM energies go beyond the current reach of the LHC and eventually surpass the reach of the HL-LHC. It is important to note that, in the event of a discovery of a Z' at the HL-LHC, the ILC will provide complementary information that will be essential in pinning down the nature of the new resonance.

8.2 Measurement of "universal" four-fermion interactions

The same analyses for probing the Z' can be recast into a set of measurements of the "universal" four-fermion interactions characterized by the parameters $\mathbf{W}$ and $\mathbf{Y}$ defined in [68, 69],

$$\mathcal{L} = \mathcal{L}_{SM} - \frac{g^2\mathbf{W}}{2m_W^2} J^a_{L\mu} J^{a\mu}_L - \frac{g'^2\mathbf{Y}}{2m_W^2} J_{Y\mu} J^\mu_Y \ , \tag{23}$$

Model	250 GeV, excl.	2 ab^{-1} disc.	500 GeV, excl.	4 ab^{-1} disc.	1 TeV, excl.	8 ab^{-1} disc.
SSM	7.8	4.9	13	8.4	22	14
ALR	9.5	6.0	17	11	25	18
χ	7.0	4.5	12	7.8	21	13
ψ	3.7	2.4	6.4	4.1	11	6.8
η	4.2	2.7	7.3	4.6	12	7.9

Table 5: Projected limits on Z' bosons in standard scenarios, from the full simulation study of $e^+e \to f\overline{f}$ described in the text. The values presented, given in TeV, are the 95% exclusion limits and the 5σ discovery limits for the successive stages of the ILC program up to 1 TeV.

$\sqrt{s}$	$\Delta\mathbf{W}$	$\Delta\mathbf{Y}$	ρ
HL-LHC	15×10^{-5}	20×10^{-5}	-0.97
ILC250	3.4×10^{-5}	2.4×10^{-5}	-0.34
ILC500	1.1×10^{-5}	0.78×10^{-5}	-0.35
ILC1000	0.39×10^{-5}	0.27×10^{-5}	-0.38
500 GeV, no beam pol.	2.0×10^{-5}	1.2×10^{-5}	-0.78

Table 6: Projections for 1-σ errors on $\mathbf{W}$ and $\mathbf{Y}$ from a 2-parameter fit to data on $e^+e \to f\overline{f}$ from the analysis described in the text. The assumed luminosities are those described in Section 2. The projection for HL-LHC (3 ab^{-1}) is based on the neutral current analysis described in [69], in particular, Fig. 2 of that paper.

where g and g' are the SM coupling constants for $SU(2)$ and $U(1)$ and $J^a_{L\mu}$, $J_{Y\mu}$ are the corresponding gauge currents. The combined results are shown in Table 6 for the three energy stages of the ILC. It is also interesting to see how the results for each flavor contribute to the final constraints. This is shown in Fig. 5. It is important to note that the beam polarisation plays a central role in this analysis to disentangle the effects from $\mathbf{W}$ and $\mathbf{Y}$. In the last line of Table 6, we show the comparable results for 4 ab^{-1} of data at 500 GeV with no beam polarisation. Not only are the results poorer, but also the correlation between $\mathbf{W}$ and $\mathbf{Y}$ is significantly increased.

8.3 Measurement of general four-fermion interactions

A more specific description of the constraints on the 4-fermion contact interactions is given by the "compositeness parameters" as defined in [16],

$$\mathcal{L} = \mathcal{L}_{SM} \pm \mathcal{L}_{LL} \pm \mathcal{L}_{LR} \pm \mathcal{L}_{RL} \pm \mathcal{L}_{RR} \tag{24}$$

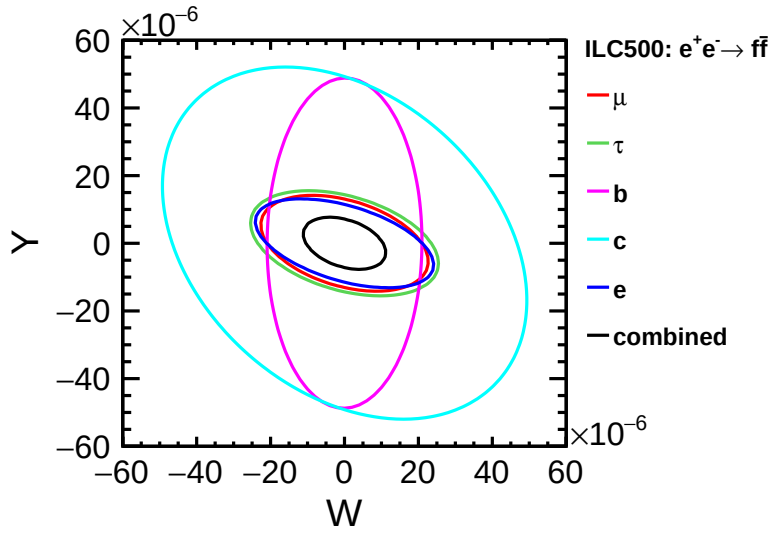

Figure 5: 68% confidence contours in the $\mathbf{W}, \mathbf{Y}$ plane for ILC at 500 GeV, from the $e^+e^- \to f\overline{f}$ analysis described in the text. The colored contours show the contributions from each flavor to the final combined limit.

with

$$\mathcal{L}_{LL} = \frac{g^2_{\rm contact}}{2\Lambda^2} \sum_j \eta^j_{LL} (\overline{e}_L \gamma_\mu e_L)(\overline{\psi}^j_L \gamma^\mu \psi^j_L),$$
$$\mathcal{L}_{LR} = \frac{g^2_{\rm contact}}{2\Lambda^2} \sum_j \eta^j_{LR} (\overline{e}_L \gamma_\mu e_L)(\overline{\psi}^j_R \gamma^\mu \psi^j_R),$$
$$\mathcal{L}_{RL} = \frac{g^2_{\rm contact}}{2\Lambda^2} \sum_j \eta^j_{RL} (\overline{e}_R \gamma_\mu e_R)(\overline{\psi}^j_L \gamma^\mu \psi^j_L),$$
$$\mathcal{L}_{RR} = \frac{g^2_{\rm contact}}{2\Lambda^2} \sum_j \eta^j_{RR} (\overline{e}_R \gamma_\mu e_R)\overline{\psi}^j_R \gamma^\mu \psi^j_R), \qquad (25)$$

where j indexes the final-state fermion flavor. At the ILC, individual $eef f$-type contact interactions can be measured for each fermion species $f = e/\mu/\tau/b/c$. In addition, the four parameters η_{LL}, η_{RR}, η_{LR} and η_{RL} can in principle be determined simultaneously using the differential cross section measurements with polarised beams. We have not yet performed a fit for all η parameters simultaneously. Instead, following the conventional approaches in [16], we give projections for the 95% exclusion limits on scale Λ for several cases of assumed η values,

$$\Lambda = \Lambda^{\pm}_{LL} \text{ for } (\eta_{LL}, \eta_{RR}, \eta_{LR}, \eta_{RL}) = (\pm 1, 0, 0, 0),$$
$$\Lambda = \Lambda^{\pm}_{RR} \text{ for } (\eta_{LL}, \eta_{RR}, \eta_{LR}, \eta_{RL}) = (0, \pm 1, 0, 0),$$

$$\Lambda = \Lambda^{\pm}_{VV} \text{ for } (\eta_{LL}, \eta_{RR}, \eta_{LR}, \eta_{RL}) = (\pm 1, \pm 1, \pm 1, \pm 1),$$
$$\Lambda = \Lambda^{\pm}_{AA} \text{ for } (\eta_{LL}, \eta_{RR}, \eta_{LR}, \eta_{RL}) = (\pm 1, \pm 1, \mp 1, \mp 1), \tag{26}$$

and $g^2_{\text{contact}}/(4\pi) = 1$. These results are presented in Table 7. The first group of limits assumes that the contact interactions are universal for all fermion species, the following groups give the results for each specific final-state fermion species. The comparable limits from LEP were about 8 TeV, that is, about 40 times the CM energy. With the increased luminosity of the ILC and the use of polarisation, we expect to be sensitive to Λ values of over 200 times the CM energy.

9 Pair production of b and t quarks

We have already pointed out in Sec. 7.2 that electroweak couplings of the top and bottom quark are of special interest for a number of reasons. In that section, we pointed to possible improvements in the Z pole coupling to $b\bar{b}$. The story of these couplings is actually more general, but that general analysis requires measurements at higher energies. As was pointed out in that section, new physics can influence heavy quark pair production both through modification of the Z and γ couplings and through the addition of four-fermion interactions mediated by new heavy gauge bosons or other particles of a strongly-coupled Higgs sector. The latter effects were discussed for b quarks in Sec. 8. It is possible to discuss the full variety of these effects in a common framework by making use of Standard Model Effective Field Theory (SMEFT). Recently, the SMEFT analysis of heavy quark electroweak couplings and the constraints from future e^+e^- experiments have been analyzed in [11, 77]. In this section, we will review some results of that work.

9.1 Measurement of the top quark mass

The top quark mass is one of the key parameters of the Standard Model and must be determined experimentally. A precise determination requires exquisite control over experimental and theoretical effects. In this section, we give a brief review of the measurement of m_t at ILC, with references to the relevant literature.

The current world average, with contributions from the Tevatron and LHC experiments is $m_t = 172.9 \pm 0.4$ GeV [16]. The experimental uncertainties are expected to improve to approximately 200 MeV at the HL-LHC. Significant theoretical work is still required to connect this quoted value of m_t to a well-defined short-distance top quark mass at that level of precision [70].

At e^+e^- colliders, a very precise measurement of the top quark mass, with a total uncertainty of approximately 50 MeV, is possible by scanning the centre-of-mass energy through the $t\bar{t}$ production threshold [71–73]. The dominant uncertainty

$\sqrt{s}$	Λ_{LL}	Λ_{RR}	Λ_{VV}	Λ_{AA}
universal Λ's				
ILC250	108	106	161	139
ILC500	189	185	280	240
ILC1000	323	314	478	403
$e^+e^- \to e^+e^-$				
ILC250	71	70	118	71
ILC500	114	132	214	135
ILC1000	236	232	376	231
$e^+e^- \to \mu^+\mu^-$				
ILC250	80	79	117	104
ILC500	134	133	198	177
ILC1000	224	222	332	296
$e^+e^- \to \tau^+\tau^-$				
ILC250	72	72	109	97
ILC500	127	126	190	168
ILC1000	215	214	321	286
$e^+e^- \to b\bar{b}$				
ILC250	78	73	103	106
ILC500	134	124	175	178
ILC1000	226	205	292	296
$e^+e^- \to c\bar{c}$				
ILC250	51	52	75	68
ILC500	90	90	130	117
ILC1000	153	151	220	199

Table 7: Projected 95% CL limits, in TeV, on the compositeness scales defined in [16], from $e^+e^- \to f\overline{f}$ analysis described in the text. In all cases, the limits from constructive (Λ^+) and destructive (Λ^-) interference are identical. The first group of numbers assumes that the Λ parameters are independent of flavor. The succeeding groups show the limits for the reactions with specific final state flavors.

is expected to be the theoretical uncertainty [74]. The theoretical expression for the threshold shape is now known to N^{3}LO order, but this still leaves a small residual theoretical uncertainty [75]. A measurement with a precision that surpasses that of the HL-LHC legacy measurement is also possible from the ILC running at $\sqrt{s}$ = 500 GeV, by taking advantage of radiative $e^+e^- \to t\bar{t}\gamma$ events [72].

9.2 Measurement of top quark electroweak couplings

The third-generation quarks play a special role in many extensions of the Standard Model. Several proposed extensions predict large deviations of the electroweak couplings of the bottom and top quark from the Standard Model value. A precise characterization of the $e^+e^- \to b\bar{b}$ and $e^+e^- \to t\bar{t}$ processes at an electron-positron collider can probe such models to very high scales. These measurements are particularly powerful in composite-Higgs models and Randall-Sundrum models with additional (warped) space-time dimensions [76,78], with the discovery potential extending up to scale of tens of TeV [77].

The $e^+e^- \to b\bar{b}$ process was studied extensively at LEP and SLC and the electroweak precision tests at the Z pole remain the most powerful constraint on the $Zb\bar{b}$ vertex today. Operation of the ILC at $\sqrt{s}$ = 250 GeV allows to determine the Z-boson and photon vector and axial couplings to b-quarks. With an integrated luminosity of 2 ab^{-1} the form factors in the general Lagrangian can be measured at the few-per-mille precision [63,80]. This implies an order of magnitude improvement with respect to the LEP combination in the determination of the right-handed coupling of the b-quark. The results at $\sqrt{s}$ =250 GeV complement the Z-pole data from the LEP/SLC experiments and GigaZ [59].

The top quark escaped scrutiny at the previous generation of electron-positrone^+e^- colliders. Measurements at the Tevatron and the LHC have characterized many of its properties. Rare associated production processes, such as $pp \to t\bar{t}X$ with X a Z-boson, photon or Higgs boson, yield direct access to the neutral-current electroweak interactions and the top quark Yukawa coupling, while single top production and top decay probe the tWb vertex. A fit of the top quark effective field theory to the LHC data has recently been performed [79]. The constraints on the operator coefficients that affect the top quark electroweak couplings are still rather weak. A combined fit of the bottom and top quark sector to LHC and LEP/SLC data yields slightly improved limits [11].

The $e^+e^- \to t\bar{t}$ process opens up at CM energies greater than twice the top quark mass. Measurements of the cross section and forward-backward asymmetry for two configurations of the beam polarisation determine the left- and right-handed couplings with sub-% precision [82]. Measuring several further observables allows us to overconstrain a global fit of all operator coefficients that directly affect these

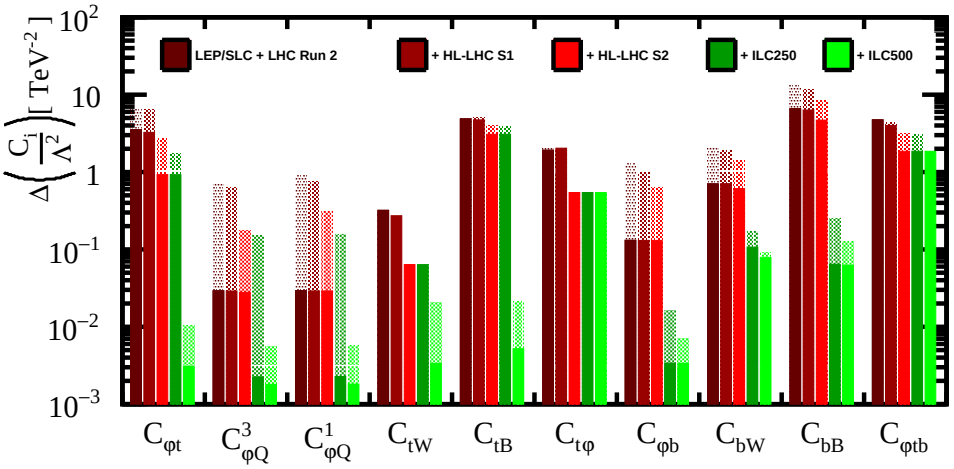

Figure 6: Prospects for the precision of the Wilson coefficients in future high-luminosity operation of the LHC and at a high-energy e^+e^- collider, from [11]. The figure shows the results of a fit to 10 coefficients of SMEFT operators that modify the electroweak couplings of the b and t quark. The solid section of the bars represents the individual constraints, where each parameter is fitted in isolation; the full length indicates the marginalized constraint in a ten-parameter fit.

couplings [10].

The prospects for the SMEFT fit of the top and bottom quark electroweak couplings are summarized in Fig. 6. This plot shows the result of a fit to a set of 10 operator coefficients corresponding to shifts in the b and t electroweak vertices. The current bounds are based on LEP/SLC data and LHC results [11]. The HL-LHC results are presented for two scenarios, S1 and S2. In the S2 scenario, LHC results are extrapolated to the complete HL-LHC luminosity assuming that experimental systematic uncertainties scale with the inverse of the integrated luminosity and that theory uncertainties improve by a factor two. The ILC prospects are based on the full simulation studies [80] and [72,82]. The effect of four-fermion operators involving b and t is not included in this fit, though those should be considered as part of a full SMEFT analysis. This case is discussed in the following section.

9.3 Measurement of the top quark Yukawa coupling

The top quark Yukawa coupling links top and Higgs physics. Several measurements of Higgs boson production and decay rates, in particular $gg \to H$ production and $H \to gg$, $H \to \gamma\gamma$ and $H \to Z\gamma$ decay, are sensitive to this coupling. Under a number of model-dependent assumptions, the Yukawa coupling can be extracted with good precision from the Higgs fit (see Section 10 and, for instance, Ref [83]).

The most robust measurement is obtained in associated production of a top quark pair and a Higgs boson. An ILC run with 4 ab^{-1} at 550 GeV is expected to reach 3.3% precision, similar to the precision envisaged in the HL-LHC S2 scenario [1]. Operation of the ILC at a centre-of-mass energy of 1 TeV improves the precision of the Yukawa coupling by a further factor two [11], to 1.6%. These results, both for ILC and LHC, are obtained from a 1-parameter fit to the $t\bar{t}h$ cross section, assuming that the other couplings contributing to this cross section have their SM values.

In the context of the SMEFT, many dimension 6 operators specifically involving b and t affect the $t\bar{t}h$ production cross section. At hadron colliders, there are about 30 distinct operators that must be considered; at e^+e^- colliders, there are 17. A robust determination of the operator coefficient $C_{t\varphi}$ that shifts the Yukawa coupling requires precise constraints on the coefficients of these other operators. A recent global fit of the top-quark sector on LHC data [79] using the complete set of operators finds that the marginalized fit result on $C_{t\varphi}$ is significantly poorer than the individual limit, since the operators that affect the QCD interactions of the top quark (in particular the $q\bar{q}t\bar{t}$ operators) are still only weakly constrained. At 500 GeV, the ILC data set still cannot determine the full set of operator coefficients needed in the e^+e^- analysis, because of degeneracy between the effects of four-fermion operators and shifts of the electroweak couplings. This degeneracy is broken by data from higher energies. The ILC including data at 1 TeV can provide a robust result in a global fit, because at that point the data with different beam polarisations and at two CM energies over-constrain the full set of relevant SMEFT parameters [11].

9.4 Requirements for b and t quark measurements

The study of the bottom and top quarks leads to several specific requirements on the accelerator and operating scenario. Beam polarisation is a key tool to disentangle the photon and Z-boson contributions to the $b\bar{b}$ and $t\bar{t}$ pair production processes [82]. The study [10] finds a 15% degradation of the overall EFT constraints without positron polarisation and a 50% degradation if no beam polarisation is available at all. Polarisation plays an even larger role in the analysis of the $e^+e^- \to b\bar{b}$ process, since final-state polarisation is accessible only through measurement of the angular distribution with polarised beams.

While the $e^+e^- \to b\bar{b}$ is accessible at the first energy stage of the ILC at 250 GeV, top quark pair production requires a CM energy of at least 350 GeV. Measurements well above threshold are desireable to escape uncertainties from threshold effects and to increase the sensitivity to axial-vector top quark couplings. The threshold for associated production of a top quark pair with a Higgs boson lies at approximately 500 GeV. Operation at still higher energy is very effective in constraining operators whose effects that grow with CM energy [10]. A robust and global characterization of all operators in the effective field theory requires an extended programme with

operation at 250 GeV, $\sqrt{s}$ = 500-550 GeV, and 1 TeV.

Third-generation quarks pose stringent requirements on the detector design and selection and reconstruction algorithm. Efficient and clean identification of jets from the hadronization of a bottom quark (b-tagging) is crucial for these analyses. The measurement of the forward-backward asymmetry in the $e^+e^- \to b\bar{b}$ analysis and in the fully hadronic final state in $e^+e^- \to t\bar{t}$ production moreover requires to distinguish jets from the fragmentation of b and $\bar{b}$ quarks. In the analysis of [63] this is achieved through a combination of vertex charge measurements and identification of kaons with low and medium momentum. The requirements of an effective b/c and $b/\bar{b}$ separation are important drivers in the design of the vertex detector. The analysis of $b\bar{b}$ and $t\bar{t}$ pair production is therefore an important benchmark for the design of the experiments.

The main challenge in the reconstruction of $t\bar{t}$ and $t\bar{t}H$ events is the large jet multiplicity. With up to eight jets in the final state, jet clustering becomes a major challenge [81]. For CM energies of 1 TeV and beyond the boost of the top quark is such that dedicated reconstruction algorithms are required [72].

10 SM EFT Higgs coupling fit at ILC

At the ILC, the most powerful method for determining the Higgs boson couplings uses a global fit of SMEFT parameters to e^+e^- observables. The default fit includes 16 dimension-6 operators, 4 SM constants and 2 parameters for Higgs to invisible and other exotic decays. By making use of the input measurements from electroweak precision observables, $e^+e^- \to WW$, Higgs observables at the HL-LHC and Higgs observables at the ILC, it is possible to fit all the parameters simultaneously. The details of the SMEFT formalism and the input measurements are explained in [4,8,84]. From the expected HL-LHC results, we use only the ratios of branching ratios for the Higgs boson decays to $\gamma\gamma$, ZZ^*, $Z\gamma$, and $\mu^+\mu^-$; these ratios have a clear model-independent interpretation. Please note that the ILC beam polarisations play a very important role. At 250 GeV, the capabilities of 2 ab^{-1} data with beam polarisations are almost as same as that of 5 ab^{-1} of data without beam polarisation. Here we only give the updated information with respect to that presented in [8].

First of all, we extend the SMEFT fit to include the measurements at 1 TeV. The estimated statistical errors for the input Higgs measurements [46] and $e^+e^- \to WW$ measurements [85] at 1 TeV based on full detector simulation studies are given in Table 12 and 13. Second, we include the improved electroweak measurements from radiative return events at 250 GeV, discussed in Sec. 6, into our default fit. Previously, in [8], we only included the factor of 10 improvement in A_ℓ in the S2*/S2 scenarios.

The improvement of precision electroweak measurements, even at the level of the

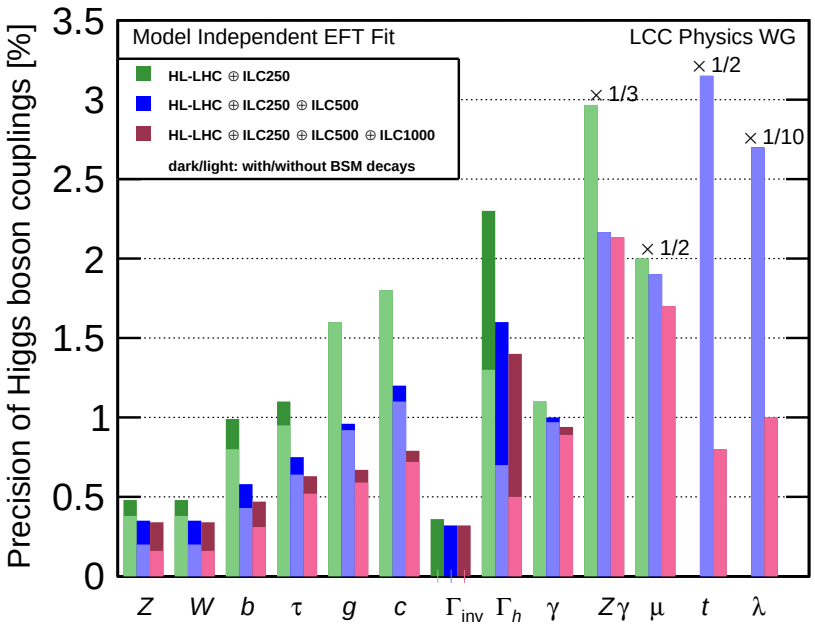

Figure 7: Projected Higgs boson coupling uncertainties for ILC250, ILC500, and ILC1000, also incorporating results expected from the HL-LHC, based on the SMEFT analysis described in the text. The darker bars show the results allowing invisible and exotic Higgs decay channels; the lighter bars assume that these BSM decays are not present. The column λ refers to the HHH coupling. In the last four columns, all bars are rescaled by the indicated factor.

radiative return analysis, allows us to take another important step. The projections in [8] and [4] made use of the assumption of lepton universality for their input values of A_ℓ and Γ_ℓ. Actually, though, the Higgs boson cross sections depend only on A_e and Γ_e. We have explained at the end of Sec. 6 that the radiative return analysis allows us to improve A_e to a level that is 10 times better than that of the current A_ℓ and to improve Γ_e to a level 15% better than that of the current Γ_ℓ. This allows us to remove the assumption that the Z couplings to the three lepton species are identical. This assumption can be separately tested in the radiative return analysis and at GigaZ, as we have explained in Secs. 6 and 7, but it is now decoupled from the fit for Higgs boson couplings.

Table 10 in Appendix A gives the updated uncertainties in the Higgs couplings for the ILC at 250 GeV and 500 GeV, and the new results at 1 TeV. Systematic errors are taken into account, as discussed in [8]. The global SMEFT fit discussed by the ECFA Higgs @ Future Colliders working group [5] made the assumption that there are no invisible or other exotic decays of the Higgs boson. To facilitate a comparison with that group, we also give the projected uncertainties with this assumption in addition

coupling	2 ab^{-1} at 250	+ 4 ab^{-1} at 500	+8 ab^{-1} at 1000
hZZ	0.35 / 0.38	0.20 / 0.20	0.16 / 0.16
hWW	0.35 / 0.38	0.20 / 0.20	0.16 / 0.16
hbb	0.79 / 0.80	0.43 /0.43	0.31 / 0.31
$h\tau\tau$	0.94 / 0.95	0.63 / 0.64	0.52 / 0.52
hgg	1.6 / 1.6	0.92 / 0.92	0.59 / 0.59
hcc	1.7 / 1.8	1.1 / 1.1	0.72 / 0.72
$h\gamma\gamma$	1.0 / 1.1	0.95 / 0.97	0.88 / 0.89
$h\gamma Z$	8.5 / 8.9	6.4 / 6.5	6.3 / 6.4
$h\mu\mu$	4.0 / 4.0	3.8 / 3.8	3.4 / 3.4
htt	—	6.3	1.6
hhh	—	27	10
Γ_{tot}	1.3 / 1.3	0.70 / 0.70	0.50 / 0.50

Table 8: Projected uncertainties in the Higgs boson couplings for the ILC250, ILC500, and ILC1000, with precision LHC input. All values are given in percent (%). The two values in each field are for fits with and without Giga-Z running. Both values are computed under the assumption of no invisible or untagged Higgs boson decays.

to the projections from our default fit. Please note that the effect is quite significant. In particular, the very small errors projected for the W, Z, and b couplings projected for ILC and other facilities depend on the assumption of no exotic Higgs decays. The projections in the table are shown graphically in Fig. 7.

Dedicated Z pole running of the ILC with GigaZ would improve the uncertainties A_e and Γ_e by a factor of 20 and 2, respectively, over current uncertainties, as we have discussed in Sec. 7. It is interesting to see how much improvement this brings in the Higgs boson couplings determined by the SMEFT fit. In Table 8 we show the effect of this improvement over the projections quoted in Table 10. It turns out that the effect is minor and disappears almost entirely for the ILC when 500 GeV data is included. A similar effect for other facilities was noted in [8]. To make the differences more visible, we have computed the projections in Table 8 using the assumption that the Higgs boson has no exotic decays.

It is worth noting that in the global SMEFT fit discussed here we include all of the the operators that are relevant to the Higgs couplings at the leading order. High-precision measurements of deviations of the Higgs couplings from the SM will need to consider also next-to-leading order effects. At this order more operators are expected to contribute, in particular the top quark operators that are discussed in Sec. 9. The Higgs and top measurements that will be available at the HL-LHC and ILC will become more intimately connected when we discuss the global SMEFT fit at NLO. Please be invited to read the paper [54].

11 Higgs self-coupling

At e^+e^- colliders, the higgs self-coupling can be measured directly in double Higgs production in the reactions $e^+e^- \to Zhh$ and $e^+e^- \to \nu\bar{\nu}hh$. The first of these reactions can be studied at the ILC at 500 GeV; the second requires higher energy to obtain a sufficient event sample. The Zhh process was analysed in [86–88] through full-simulation studies of this process in the decay modes $hh \to (b\bar{b})(b\bar{b})$ and $hh \to (b\bar{b})(W + W^-)$. For a 4 ab^{-1} data set, these results extrapolate to a precision of 27% [89], if the self-coupling has a value close to the SM expectation. The extraction of the self-coupling was based on a 1-parameter fit varying the Higgs self-coupling only. But also, it was shown in [84] that this uncertainty is essentially unchanged in the context of a SMEFT analysis including all possible dimension-6 operators, since the additional relevant operator coefficients are strongly constrained by single-h measurements at the ILC.

The same framework has been used to perform full-simulation studies of the cross section measurement for $e^+e^- \to \nu\bar{\nu}hh$ at 1 TeV, again using the $hh \to (b\bar{b})(b\bar{b})$ and $hh \to (b\bar{b})(W^+W^-)$ decay modes [90]. Extrapolating these results to a data set of 8 ab^{-1}, we find an estimated precision of 10% on the Higgs self-coupling [8], again for the case in which the self-coupling is close to the SM value. The authors of [84] believe that this uncertainty estimate will also turn out to be highly model-independent, though the analysis has not yet been completed.

In theoretical models, especially in models of electroweak baryogenesis, the Higgs self-coupling can be enhanced over its SM value by a factor of 2. It is therefore important to take account of the fact that the uncertainty on the Higgs self-coupling varies with the assumed value of this coupling. In all processes, the digram containing the self-coupling appears in interference with other SM diagrams. The uncertainty on the Higgs self-coupling decreases in the case of constructive interference but increases in the case of destructive interference. (The latter situation is well known for $gg \to hh$ at hadron colliders.) An advantage of e^+e^- collider studies is that the two reactions Zhh and W fusion reactions have opposite signs for the interference term. This effect is shown in Fig. 8, which shows that, whether the self-coupling increases or decreases from its SM value, the combination of the two e^+e^- reactions shows robust performance, reaching precisions below 15% in the combination for any values of the self-coupling larger than 0.4 times the SM value.

It should be emphasized, both for $t\bar{t}h$ production and for both modes of hh production, that the numbers we have quoted here are based on our current reconstruction algorithms applied to full-simulation data. In all three cases, the efficiencies of these algorithms leave substantial room for improvement. We thus expect that further study and especially experience will real data will improve these estimates substantially [88].

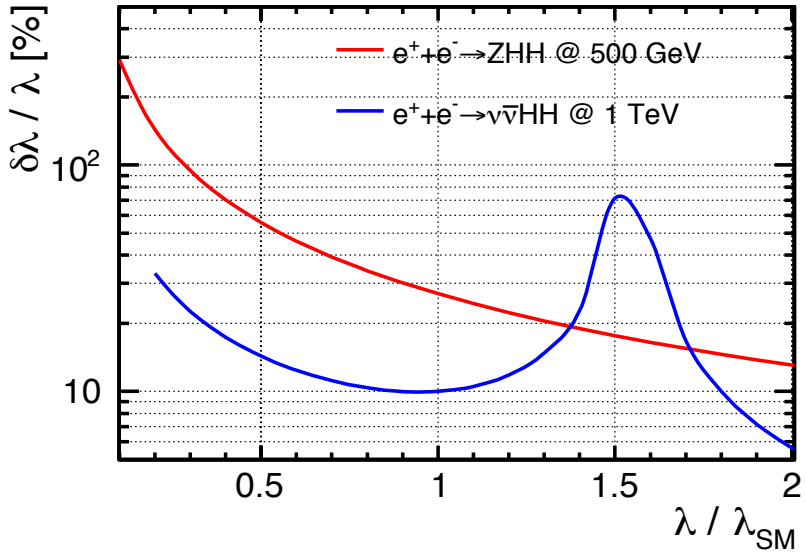

Figure 8: The expected precisions of the Higgs self-coupling λ at the ILC as a function of the assumed value of λ, for the reactions $e^+e^- \to Zhh$ (red) and for $e^+e^- \to \nu\bar{\nu}hh$ (blue). The luminosities assumed are: 4 ab^{-1} at 500 GeV and 4 ab^{-1} with $(P_{e^-}, P_{e^+}) = (-80\%, +20\%)$ at 1 TeV.

12 Conclusion

In this paper, we have described the potential of the ILC to improve precision electroweak measurements and other precision probes of the Standard Model.

For precision electroweak measurements, we have shown that the capabilities of the ILC are very powerful, both using data from running at 250 GeV and especially from a dedicated GigaZ stage of running at the Z pole. The availability of polarised beams, both for electrons and for positrons, is an important part of this story. With few exceptions, the limiting factor in precision electroweak measurements is not statistics but rather the control of systematic errors. We have explained how the ILC experiments will control the effective polarisation of beams to the level of $(3-5)\times 10^{-4}$ and will transfer this level of precision to the most important electroweak observables.

We have also reviewed and updated the ILC capabilities for studies of fermion pair production, including b and t quark production. The ILC will determine the top quark mass to a precision of 2×10^{-4}. It will also give strong bounds on the presence of Z' resonances and contact interactions due to new physics at high energies. The availability of polarised beams will make these constraints very specific in terms of the flavor and helicity structure of the operators probed—or, in the event that a deviation from the SM is discovered, will make the origin of the corrections to the

SM very clear.

Finally, we have reviewed the ILC capabilities for the measurement of Higgs boson couplings, including the top quark Yukawa coupling and the Higgs boson self-coupling. As we learn more about the ILC capabilities for other measurements, the projection that the ILC will measure the couplings of the Higgs boson visible in Higgs decay to precisions below 1% remains robust.

Acknowledgements

We thank the members of the Higgs@Future Colliders working group and the BSM working group of the current study for the European Strategy for Particle Physics for stimulating the writing of this paper, and for many discussions of the analyses presented here. We are especially grateful to Juan Alcaraz, Jorge de Blas, Beate Heinemann, Aleandro Nisati, Andrea Wulzer, and Kaoru Yokoya for discussions of this material and to Alain Blondel and Patrick Janot for useful correspondence. We are grateful to many funding agencies around the world for supporting the research reported here and the preparation of this document. Among these are: the Deutsche Forschungsgemeinschaft (DFG, German Research Foundation) under Germanys Excellence Strategy EXC 2121 "Quantum Universe" 390833306, the Generalitat Valenciana under grant PROMETEO 2018/060 and the Spanish national program for particle physics under grant FPA2015-65652-C4-3-R, the Japan Society for the Promotion of Science (JSPS) under Grants-in-Aid for Science Research 15H02083, 16H02173, and 16H02176, the US National Science Foundation under grant PHY-1607262, and the US Department of Energy under contracts DE–AC02–76SF00515, DE–AC05–06OR23177, and DE–SC0017996.

A ILC projected uncertainties on precision electroweak observables and Higgs boson couplings

Table 9: Projected precision of precision electroweak quantities expected from the ILC. Precisions are given as *relative* errors ($\delta A = \Delta A/A$) in units of 10^{-4}. The first two columns list the quantities and their SM values. The third column gives the current uncertainty [16]. The fourth and fifth columns show the statistical and systematic errors expected from a GigaZ run of the ILC. The fifth and sixth columns show the statistical and systematic errors expected from 250 GeV running of the ILC from measurements of $e^+e^- \to Z\gamma$. In cases where the statistical uncertainty is negligible with respect to the systematic uncertainty, or vice versa, the smaller element of the table is left blank. Boxes in which there is no improvement are marked "-". Footnote symbols show the source of the dominant systematic error: † acceptance; $^\circ$ energy scale; * beam polarisation; $^+$ flavor tag; $^\#$ multiple effects, improved from SLC. The errors on g_L, g_R are computed from those on R, A, and $\Gamma_Z(had)$.

Table 10: Projected uncertainties in the Higgs boson couplings for the ILC250, ILC500, and ILC1000, with precision LHC input. All values are *relative* errors, given in percent (%). The columns labelled "full" refer to a 22-parameter fit including the possibility of invisible and exotic Higgs boson decays. The columns labelled "no BSM" refer to a 20-parameter fit including only decays modes present in the SM. The definition of a Higgs coupling uncertainty, for the purpose of this table, is half the fractional uncertainty in the corresponding Higgs boson partial width. The bottom lines give, for reference, the projected uncertainties in the Higgs boson total width and the 95% confidence limits on the Higgs boson invisible width. The analysis, which applies Effective Field Theory as described in the text, is highly model-independent. The ILC250 does not have direct sensitivity to the htt and hhh couplings; thus no model-independent values are given in these lines. The projections presented for these couplings in the ILC500 and ILC500 columns are based on 1-parameter fits to the $ht\bar{t}$ and hh production cross sections.

Quantity	Value	current	GigaZ		ILC250	
		$\delta[10^{-4}]$	$\delta_{stat}[10^{-4}]$	$\delta_{sys}[10^{-4}]$	$\delta_{stat}[10^{-4}]$	$\delta_{sys}[10^{-4}]$
boson properties						
m_W	80.379	1.5	-	-		0.3 $^{\circ}$
m_Z	91.1876	0.23	-	-	-	-
Γ_Z	2.4952	9.4		4. $^{\circ}$	-	-
$\Gamma_Z(had)$	1.7444	11.5		4. $^{\circ}$	-	-
Z-e couplings						
$1/R_e$	0.0482	24.	2.	5 †	5.5	10 $^{+}$
A_e	0.1513	139.	1	5. *	9.5	3. *
g_L^e	-0.632	16.	1.0	3.2	2.8	7.6
g_R^e	0.551	18.	1.0	3.2	2.9	7.6
Z-ℓ couplings						
$1/R_\mu$	0.0482	16.	2.	2. †	5.5	10 $^{+}$
$1/R_\tau$	0.0482	22.	2.	4. †	5.7	10 $^{+}$
A_μ	0.1515	991.	2.	5 *	54.	3. *
A_τ	0.1515	271.	2.	5. *	57.	3 *
g_L^μ	-0.632	66.	1.0	2.3	4.5	7.6
g_R^μ	0.551	89.	1.0	2.3	5.5	7.6
g_L^τ	-0.632	22.	1.0	2.8	4.7	7.6
g_R^τ	0.551	27.	1.0	3.2	5.8	7.6
Z-b couplings						
R_b	0.2163	31.	0.4	7. $^{\#}$	3.5	10 $^{+}$
A_b	0.935	214.	1.	5. *	5.7	3 *
g_L^b	-0.999	54.	0.32	4.2	2.2	7.6
g_R^b	0.184	1540	7.2	36.	41.	23.
Z-c couplings						
R_c	0.1721	174.	2.	30 $^{\#}$	5.8	50 $^{+}$
A_c	0.668	404.	3.	$5^{*} \oplus 5^{\#}$	21.	3 *
g_L^c	0.816	119.	1.2	15.	5.1	26.
g_R^c	-0.367	416.	3.1	17.	21.	26.

Table 9: Projected precision of precision electroweak quantities expected from the ILC. Precisions are given as *relative* errors ($\delta A = \Delta A/A$) in units of 10^{-4}. Please see the text of Appendix A for further explanation of this table.

	ILC250		ILC500		ILC1000	
coupling	full	no BSM	full	no BSM	full	no BSM
hZZ	0.48	0.38	0.35	0.20	0.34	0.16
hWW	0.48	0.38	0.35	0.20	0.34	0.16
hbb	0.99	0.80	0.58	0.43	0.47	0.31
$h\tau\tau$	1.1	0.95	0.75	0.64	0.63	0.52
hgg	1.6	1.6	0.96	0.92	0.67	0.59
hcc	1.8	1.8	1.2	1.1	0.79	0.72
$h\gamma\gamma$	1.1	1.1	1.0	0.97	0.94	0.89
$h\gamma Z$	8.9	8.9	6.5	6.5	6.4	6.4
$h\mu\mu$	4.0	4.0	3.8	3.8	3.4	3.4
htt	—	—	6.3	6.3	1.6	1.6
hhh	—	—	27	27	10	10
Γ_{tot}	2.3	1.3	1.6	0.70	1.4	0.50
Γ_{inv}	0.36	—	0.32	—	0.32	—

Table 10: Projected uncertainties in the Higgs boson couplings for the ILC250, ILC500, and ILC1000, with precision LHC input. All values are *relative* errors, given in percent (%). The columns labelled "full" refer to a 22-parameter fit including the possibility of invisible and exotic Higgs boson decays. The columns labelled "no BSM" refer to a 20-parameter fit including only decays modes present in the SM. Please see the text of Appendix A for further explanation of this table.

B Uncertainties on observables used as inputs to the ILC Higgs boson coupling projections

Table 11: Values and uncertainties for precision electroweak observables used in this paper. Current values are taken from [16], except for the averaged value of A_ℓ, which corresponds to the averaged value of $\sin^2\theta_{eff}$ in [17]. The best fit values are those of the fit in [16]. For the purpose of fitting Higgs boson couplings as described in Sec. 10, we use expected improvements from the ILC in the uncertainty on the Higgs mass, from [8], and improvements on the precision electroweak observables and W properties explained in this paper.

Table 12 Projected statistical errors, quoted as relative errors in %, for Higgs boson measurements input to our fits. The errors are quoted for luminosity samples of 250 fb^{-1} for e^+e^- beams with -80% electron polarisation and +30% positron polarisation, in the top half of the table, and with +80% electron polarisation and -30% positron polarisation, in the bottom half of the table—except that the values in the column for 1000 GeV are given for $\mp 80\%/\pm 20\%$ e^-/e^+ polarization. Except for the first and last segments of each set, these are measurments of $\sigma \cdot BR$, relative to the Standard Model expectation. The top lines gives the error for the total cross section

relative to the Standard Model and the 95% confidence upper limit on the branching ratio for Higgs to invisible decays. The bottom lines in each half give the expected errors on the a and b parameters and their correlation (all in %) for $e^+e^- \to Zh$ (see [84]). All error estimates in this table are based on full simulation, or on the extrapolation of full simulation results to different energies or polarization settings.

Table 13: Projected statistical errors, in %, for $e^+e^- \to W^+W^-$ measurements input to our fits. The errors are derived from a 3-parameter fit, assuming $SU(2)\times U(1)$ invariance, to the quantities g_{1Z}, κ_A, λ_A characterizing triple gauge bosons anomalous couplings. These errors are then interpreted in SMEFT according to the prescription given in [84]. The errors are quoted for luminosity samples of 500 fb^{-1} divided equally between beams with -80% electron polarisation and +30% positron polarisation and beams with +80% electron polarisation and -30% positron polarisation. The last three lines give the correlation coefficients, also in %. All error estimates in this table are based on full simulation, or on the extrapolation of full simulation results to different energies.

Observable	current value	current σ	ILC250 σ	GigaZ σ	SM best fit value
$\alpha^{-1}(m_Z^2)$	128.9220	0.0178			(same)
G_F (10^{-10} GeV^{-2})	1166378.7	0.6			(same)
m_W (MeV)	80385	15	2.5		80361
m_Z (MeV)	91187.6	2.1			91.1880
m_h (MeV)	125090	240	15		125110
A_ℓ	0.14696	0.0013	0.00015	0.000075	0.147937
Γ_e (MeV)	83.919	0.105	0.072	0.047	83.995
Γ_Z (MeV)	2495.2	2.3		1.	2.4943
$BR(W \to e\nu)$ (%)	10.71	0.16	0.011		10.86

Table 11: Values and uncertainties for precision electroweak observables used in this paper. Please see the text of Appendix B for the explanation of this table.

-80% e^- polarisation, +30% e^+ polarisation:

	250 GeV		350 GeV		500 GeV		1000 GeV
	Zh	$\nu\bar{\nu}h$	Zh	$\nu\bar{\nu}h$	Zh	$\nu\bar{\nu}h$	$\nu\bar{\nu}h$
σ	2.0		1.8		4.2		
$h \to invis.$	0.86		1.4		3.4		
$h \to b\bar{b}$	1.3	8.1	1.5	1.8	2.5	0.93	1.0
$h \to c\bar{c}$	8.3		11	19	18	8.8	6.2
$h \to gg$	7.0		8.4	7.7	15	5.8	4.6
$h \to WW$	4.6		5.6	5.7	7.7	3.4	3.2
$h \to \tau\tau$	3.2		4.0	16	6.1	9.8	6.2
$h \to ZZ$	18		25	20	35	12	8.2
$h \to \gamma\gamma$	34		39	45	47	27	17
$h \to \mu\mu$	72		87	160 *	120 *	100	62
a	7.6		2.7		4.0		
b	2.7		0.69		0.70		
$\rho(a,b)$	-99.17		-95.6		-84.8		

+80% e^- polarisation, -30% e^+ polarisation:

	250 GeV		350 GeV		500 GeV		1000 GeV
	Zh	$\nu\bar{\nu}h$	Zh	$\nu\bar{\nu}h$	Zh	$\nu\bar{\nu}h$	$\nu\bar{\nu}h$
σ	2.0		1.8		4.2		
$h \to invis.$	0.61		1.3		2.4		
$h \to b\bar{b}$	1.3	33	1.5	7.5	2.5	3.8	3.7
$h \to c\bar{c}$	8.3		11	79	18	36	23
$h \to gg$	7.0		8.4	32	15	24	17
$h \to WW$	4.6		5.6	24	7.7	14	12
$h \to \tau\tau$	3.2		4.0	66	6.1	40	23
$h \to ZZ$	18		25	81	35	48	30
$h \to \gamma\gamma$	34		39	180	47	110	62
$h \to \mu\mu$	72		87	670	120	420	230
a	9.1		3.1		4.2		
b	3.2		0.79		0.75		
$\rho(a,b)$	-99.39		-96.6		-86.5		

Table 12: Projected statistical errors, quoted as relative errors in %, for Higgs boson measurements input to our fits. The errors are quoted for luminosity samples of 250 fb^{-1} for e^+e^- beams with -80% electron polarisation and +30% positron polarisation, in the top half of the table, and with +80% electron polarisation and -30% positron polarisation, in the bottom half of the table. Please see the text of Appendix B for further explanation of this table.

	250 GeV W^+W^-	350 GeV W^+W^-	500 GeV W^+W^-	1000 GeV W^+W^-
g_{1Z}	0 .062	0.033	0.025	0.0088
κ_A	0.096	0.049	0.034	0.011
λ_A	0.077	0.047	0.037	0.0090
$\rho(g_{1Z}, \kappa_A)$	63.4	63.4	63.4	63.4
$\rho(g_{1Z}, \lambda_A)$	47.7	47.7	47.7	47.7
$\rho(\kappa_A, \lambda_A)$	35.4	35.4	35.4	35.4

Table 13: Projected statistical errors, in %, for $e^+e^- \to W^+W^-$ measurements input to our fits. The errors are quoted for luminosity samples of 500 fb^{-1} divided equally between beams with -80% electron polarisation and +30% positron polarisation and brams with +80% electron polarisation and -30% positron polarisation. Please see the text of Appendix B for further explanation of this table.

References

[1] M. Cepeda *et al.* [HL/HE LHC WG2 group], [arXiv:1902.00134 [hep-ph]].

[2] S. Dawson, *et al.*, in *Proceedings of the 2013 Community Summer Study on the Future of U.S. Particle Physics*, N. Graf, M. E. Peskin, and J. Rosner, eds. http://www.slac.stanford.edu/econf/C1307292/ [arXiv:1310.8361 [hep-ex]].

[3] G. Durieux, C. Grojean, J. Gu and K. Wang, JHEP **09**, 014 (2017) [arXiv:1704.02333 [hep-ph]].

[4] T. Barklow, K. Fujii, S. Jung, R. Karl, J. List, T. Ogawa, M. E. Peskin and J. Tian, Phys. Rev. D **97**, 053003 (2018) [arXiv:1708.08912 [hep-ph]].

[5] J. de Blas, M. Cepeda, J. D'Hondt, R. Ellis, C. Grojean, B. Heinemann, F. Maltoni, A. Nisati, E. Petit, R. Rattazzi and W. Verkerke, [arXiv:1905.03764 [hep-ph]].

[6] J. de Blas, G. Durieux, C. Grojean, J. Gu and A. Paul, [arXiv:1907.04311 [hep-ph]].

[7] T. Behnke, *et al.*, "The International Linear Collider Technical Design Report - Volume 4: Detectors," [arXiv:1306.6329 [physics.ins-det]].

[8] P. Bambade, *et al.*, "The International Linear Collider: A Global Project," [arXiv:1903.01629 [hep-ex]].

[9] T. Barklow, J. Brau, K. Fujii, J. Gao, J. List, N. Walker and K. Yokoya, arXiv:1506.07830 [hep-ex].

[10] G. Durieux, M. Perelló, M. Vos and C. Zhang, JHEP **10**, 168 (2018) [arXiv:1807.02121 [hep-ph]].

[11] G. Durieux, A. Irles, V. Miralles, A. Peñuelas, R. Pöschl, M. Perelló and M. Vos, [arXiv:1907.10619 [hep-ph]].

[12] C. Adolphsen *et al.*, "The International Linear Collider Technical Design Report - Volume 3.I: Accelerator R&Din the Technical Design Phase," [arXiv:1306.6353 [physics.acc-ph]].

[13] C. Adolphsen *et al.*, "The International Linear Collider Technical Design Report - Volume 3.II: Accelerator Baseline Design," arXiv:1306.6328 [physics.acc-ph].

[14] G. Moortgat-Pick *et al.*, Phys. Rept. **460**, 131 (2008) [hep-ph/0507011].

[15] K. Fujii *et al.* [arXiv:1801.02840 [hep-ph]].

[16] M. Tanabashi *et al.* [Particle Data Group], "Review of Particle Physics," Phys. Rev. D **98**, 030001 (2018)

[17] S. Schael *et al.* [ALEPH and DELPHI and L3 and OPAL and SLD Collaborations and LEP Electroweak Working Group and SLD Electroweak Group and SLD Heavy Flavour Group], Phys. Rept. **427**, 257 (2006) [hep-ex/0509008].

[18] N. Walker, "ILC possibilities at Z and W," priv. note March 15, 2016.

[19] K. Yokoya, K. Kubo and T. Okugi, arXiv:1908.08212 [physics.acc-ph].

[20] S. Boogert *et al.*, "Polarimeters and Energy Spectrometers for the ILC Beam Delivery System," JINST **4**, P10015 (2009) [arXiv:0904.0122 [physics.ins-det]].

[21] B. Vormwald, J. List and A. Vauth, "A calibration system for Compton polarimetry at e^+e^- linear colliders," JINST **11**, P01014 (2016) [arXiv:1509.03178 [physics.ins-det]].

[22] J. List, A. Vauth and B. Vormwald, JINST **10**, P05014 (2015) [arXiv:1502.06955 [physics.ins-det]].

[23] I. B. Mordechai and G. Alexander, in *Proceedings of the 3rd Linear Collider Forum*, G. Moortgat-Pick, ed. DESY-PROC-2013-02 (2013).

[24] M. Beckmann, J. List, A. Vauth and B. Vormwald, "Spin Transport and Polarimetry in the Beam Delivery System of the International Linear Collider," JINST **9**, P07003 (2014) [arXiv:1405.2156 [physics.acc-ph]].

[25] R. Karl, "From the Machine-Detector Interface to Electroweak Precision Measurements at the ILC — Beam-Gas Background, Beam Polarisation and Triple Gauge Couplings," University of Hamburg Ph.D. thesis, DESY-THESIS-2019-018 (2019). ,

[26] A. Blondel, "A Scheme to Measure the Polarisation Asymmetry at the Z Pole in LEP," Phys. Lett. B **202**, 145 (1988); Erratum: [Phys. Lett. **208** (1988) 531].

[27] K. Mönig, "The Use of positron polarization for precision measurements," LC-PHSM-2000-059.

[28] I. Marchesini, "Triple gauge couplings and polarisation at the ILC and leakage in a highly granular calorimeter," University of Hamburg Ph.D. thesis, DESY-THESIS-2011-044.

[29] G. Wilson, "Investigating Precision In-Situ $\sqrt{s}$ Determination with $\mu^+\mu^-(\gamma)$ Events". https://agenda.linearcollider.org/event/5840/contributions/26233/.

[30] G. Wilson, "Prospects for precision momemntum scale calibration," presentation at AWLC 2014, https://agenda.linearcollider.org/event/6301/contributions/29525/attachments/24486/37868/MomentumScaleStud_ConvertedByMe.pdf.

[31] S. Poss and A. Sailer, "Luminosity Spectrum Reconstruction at Linear Colliders," Eur. Phys. J. C **74**, 2833 (2014) [arXiv:1309.0372 [physics.ins-det]].

[32] C. Grah and A. Sapronov, "Beam parameter determination using beamstrahlung photons and incoherent pairs," JINST **3**, P10004 (2008).

[33] M. Habermehl, "Dark Matter at the International Linear Collider," University of Hamburg Ph.D. thesis, DESY-THESIS-2018-039 (2018).

[34] I. Bozovic-Jelisavcic, S. Lukic, M. Pandurovic and I. Smiljanic, "Luminosity measurement at ILC," JINST **8**, P08012 (2013) [arXiv:1304.4082 [physics.acc-ph]].

[35] M. Baak *et al.*, "Working Group Report: Precision Study of Electroweak Interactions," arXiv:1310.6708 [hep-ph].

[36] K. Hagiwara, R. D. Peccei, D. Zeppenfeld and K. Hikasa, Nucl. Phys. B **282**, 253 (1987).

[37] G. Abbiendi *et al.* [OPAL Collaboration], Eur. Phys. J. C **26**, 321 (2003) [hep-ex/0203026].

[38] G. W. Wilson, arXiv:1603.06016 [hep-ex].

[39] Z. Kunszt *et al.*, hep-ph/9602352.

[40] W. J. Stirling, Nucl. Phys. B **456**, 3 (1995) [hep-ph/9503320].

[41] A. Heister *et al.* [ALEPH Collaboration], Eur. Phys. J. C **38**, 147 (2004).

[42] J. Abdallah *et al.* [DELPHI Collaboration], Eur. Phys. J. C **34**, 127 (2004) [hep-ex/0403042].

[43] P. Achard *et al.* [L3 Collaboration], Phys. Lett. B **600**, 22 (2004) [hep-ex/0409016].

[44] G. Abbiendi *et al.* [OPAL Collaboration], Eur. Phys. J. C **52**, 767 (2007) [arXiv:0708.1311 [hep-ex]].

[45] A. Blondel, A. Freitas, J. Gluza, T. Riemann, S. Heinemeyer, S. Jadach and P. Janot, [arXiv:1901.02648 [hep-ph]].

[46] D. M. Asner *et al.*, arXiv:1310.0763 [hep-ph].

[47] [ALEPH Collaboration], hep-ex/9810047.

[48] Takayuki Ueno, "A simulation study on measurement of the polarisation asymmetry A_{LR} using the initial state radiation at the ILC with center-of-mass energy of 250 GeV", Tohoku University Masters Thesis, 2019.

[49] P. C. Rowson, D. Su and S. Willocq, Ann. Rev. Nucl. Part. Sci. **51**, 345 (2001) [hep-ph/0110168].

[50] S. Bilokin, A. Irles, R. Pöschl and F. Richard, "Measurement of b quark EW couplings at ILC250", In preparation.

[51] S. Bilokin, A. Irles, R. Pöschl and F. Richard, "Measurement of c quark EW couplings at ILC250", In preparation.

[52] D. Jeans, "ILD Benchmark Analysis for $e^+e^- \to \tau^+\tau^-$", ILD note in preparation.

[53] Y. Deguchi, H. Yamashiro, T. Suehara, T. Yoshioka, K. Fujii and K. Kawagoe, arXiv:1902.05245 [hep-ex].

[54] S. Jung, J. Lee, M. Perelló, J. Tian, and M. Vos, "Higgs and Top Precision at Lepton Colliders with Renormalization Operator Mixing", paper in preparation.

[55] J. Aguilar-Saavedra *et al.* [ECFA/DESY LC Physics Working Group], [arXiv:hep-ph/0106315 [hep-ph]].

[56] A. Abada *et al.* [FCC], Eur. Phys. J. ST **228**, 261 (2019)

[57] P. Eberhard *et al.*, in "Z Physics at LEP 1", Vol. 1, G. Altarelli, R. Kleiss, and C. Verzegnassi, eds. CERN 89-08 (1989).

[58] M. Vincter, presentation at FCC Week 2019, https://indico.cern.ch/event/727555/contributions/3437129/.

[59] A. Irles, R. Pschl, F. Richard, and H. Yamamoto, [arXiv:1905.00220 [hep-ex]].

[60] K. Abe *et al.* [SLD], Phys. Rev. D **71**, 112004 (2005) [arXiv:hep-ex/0503005 [hep-ex]].

[61] K. Abe *et al.* [SLD], Phys. Rev. Lett. **94**, 091801 (2005) [arXiv:hep-ex/0410042 [hep-ex]].

[62] G. Abbiendi *et al.* [OPAL], Eur. Phys. J. C **13**, 1 (2000) [arXiv:hep-ex/9908001 [hep-ex]].

[63] S. Bilokin, R. Pöschl and F. Richard, arXiv:1709.04289 [hep-ex].

[64] T. Takeuchi, A. K. Grant and J. L. Rosner, [arXiv:hep-ph/9409211 [hep-ph]].

[65] A. Djouadi, G. Moreau and F. Richard, Nucl. Phys. B **773**, 43 (2007) [arXiv:hep-ph/0610173 [hep-ph]].

[66] S. Funatsu, H. Hatanaka, Y. Hosotani, and Y. Orikasa, Phys. Lett. B **775**, 297 (2017) [arXiv:1705.05282 [hep-ph]].

[67] J. Yoon and M. E. Peskin, [arXiv:1811.07877 [hep-ph]].

[68] R. Barbieri, A. Pomarol, R. Rattazzi and A. Strumia, Nucl. Phys. B **703**, 127 (2004) [arXiv:hep-ph/0405040 [hep-ph]].

[69] M. Farina, G. Panico, D. Pappadopulo, J. T. Ruderman, R. Torre and A. Wulzer, Phys. Lett. B **772**, 210 (2017) [arXiv:1609.08157 [hep-ph]].

[70] P. Azzi *et al.* [HL-LHC Collaboration and HE-LHC Working Group], arXiv:1902.04070 [hep-ph].

[71] F. Simon, arXiv:1902.07246 [hep-ex].

[72] H. Abramowicz *et al.* [CLICdp Collaboration], arXiv:1807.02441 [hep-ex].

[73] M. Vos *et al.*, arXiv:1604.08122 [hep-ex].

[74] F. Simon, PoS ICHEP **2016**, 872 (2017) [arXiv:1611.03399 [hep-ex]].

[75] M. Beneke, Y. Kiyo, P. Marquard, A. Penin, J. Piclum and M. Steinhauser, Phys. Rev. Lett. **115**, 192001 (2015) [arXiv:1506.06864 [hep-ph]].

[76] F. Richard, arXiv:1403.2893 [hep-ph].

[77] G. Durieux and O. Matsedonskyi, JHEP **1901**, 072 (2019) [arXiv:1807.10273 [hep-ph]].

[78] K. Agashe, R. Contino, L. Da Rold and A. Pomarol, Phys. Lett. B **641**, 62 (2006). [hep-ph/0605341].

[79] N. P. Hartland, F. Maltoni, E. R. Nocera, J. Rojo, E. Slade, E. Vryonidou and C. Zhang, JHEP **1904**, 100 (2019) [arXiv:1901.05965 [hep-ph]].

[80] A. Irles, R. Pöschl, F. Richard, ILD-NOTE-2019 (to appear).

[81] M. Boronat, J. Fuster, I. Garcia, P. Roloff, R. Simoniello and M. Vos, Eur. Phys. J. C **78**, 144 (2018) [arXiv:1607.05039 [hep-ex]].

[82] M. S. Amjad *et al.*, Eur. Phys. J. C **75**, 512 (2015) [arXiv:1505.06020 [hep-ex]].

[83] S. Boselli, R. Hunter, and A. Mitov, arXiv:1805.12027 [hep-ph].

[84] T. Barklow, K. Fujii, S. Jung, M. E. Peskin and J. Tian, Phys. Rev. D **97**, 053004 (2018) [arXiv:1708.09079 [hep-ph]].

[85] A. Rosca, Nucl. Part. Phys. Proc. **273-275**, 2226 (2016).

[86] Y. Takubo, arXiv:0907.0524 [hep-ph].

[87] J. Tian, K. Fujii and Y. Gao, arXiv:1008.0921 [hep-ex].

[88] C. F. Dürig, "Measuring the Higgs Self-Coupling at the International Linear Collider," University of Hamburg Ph.D. thesis, DESY-THESIS-2016-027 (2016).

[89] K. Fujii *et al.*, arXiv:1506.05992 [hep-ex].

[90] J. Tian *et al.* [ILD Collaboration], PoS EPS-**HEP2013**, 316 (2013) [arXiv:1311.6528 [hep-ph]].